

# Structural Engineering and Coupling of Two-Dimensional Transition Metal Compounds for Micro-Supercapacitor Electrodes

Waqas Ali Haider, Muhammad Tahir, Liang He,\* H. A. Mirza, Ruiqi Zhu, Yulai Han,\* and Liqiang Mai\*



Cite This: <https://dx.doi.org/10.1021/acscentsci.0c01022>



Read Online

ACCESS |

 Metrics & More

 Article Recommendations

**ABSTRACT:** The development of portable, wearable, and miniaturized integrated electronics has significantly promoted the immense desire for planar micro-supercapacitors (MSCs) among the extremely competitive energy storage devices. However, their energy density is still insufficient owing to the low electrochemical performance of conventional electrode materials. Compared with their bulk counterparts, the large specific surface area and fast ion transport with efficient intercalation of two-dimensional (2D) transition metal compounds have spurred the research platforms for their exploitation in the creation of high-performance MSCs. This Outlook presents a systematic summary of cutting-edge research on atomically thin, layered structures of transition metal dichalcogenides, MXenes, and transition metal oxides/hydroxides. Special emphasis is given to the rapid and durable storage of ions, benefiting from the low ion diffusion barriers of host interlayer spaces. Moreover, various strategies have been described to circumvent the structural damage due to the volume change and simultaneously evincing remarkable electronic properties.



## 1. INTRODUCTION

The sustained progression of portable technologies has driven the desire for the development of micro-power-sources which are potentially able to be integrated into miniaturized systems for medical, telecommunication, and other microelectronic devices.<sup>1,2</sup> Although thin-film Li-ion microbatteries (MBs) are dominant due to their high energy density ( $\sim 1 \text{ mW h cm}^{-2}$ ), their short lifetime (500–10 000 cycles) and low power density ( $< 5 \text{ mW cm}^{-2}$ ) inhibit their applications in systems where battery replacement is infeasible, and huge energy spikes are required.<sup>3–5</sup> Micro-supercapacitors (MSCs) are safe alternative energy-storage solutions which manifest a longer lifetime ( $> 100\,000$  cycles) and provide high power density ( $> 10 \text{ mW cm}^{-2}$ ) with rapid charge/discharge capabilities.<sup>6–8</sup> MSCs with the conventional electric double layer (EDL) mechanism exhibit low energy density ( $< 0.1 \text{ mW h cm}^{-2}$ ) owing to their intrinsic electrostatic charge storage that requires large surface area and pore sizes.<sup>9,10</sup> Although the capacitance can be increased by employing an active electrode material with large volume, that consequently increases the size of the cell to an undesired extent.<sup>11</sup> Contrary to EDL, the pseudocapacitive mechanism of charge storage exhibits elevated energy density and specific capacitance via a rapid repeatable redox reaction among the active electrode material and electrolyte.<sup>12,13</sup> Typically, EDL and pseudocapacitance occur together in MSCs; however, one of them becomes dominant based on the interaction of electrode material with electrolyte ions.<sup>14</sup> The redox reaction involves the exchange of charges across the double layer rather than creating a cloud of immovable charges around the electrode material.<sup>15</sup> The

charge storage of pseudocapacitive materials has a linear reliance on the range of applied potential and tendency of oxidation and reduction, though the redox reaction can continuously change the oxidation states of electrode cations, which eventually degrades the cycling performance of the pseudocapacitor.

The aforementioned challenges cause a driving force toward the exploration of electroactive materials to achieve efficient charge transfer between electrode and electrolyte. Materials based on transition metal compounds have been enthusiastically investigated for charge storage because of their variable oxidation states, which enable transition metal cations to actively participate in the Faradaic charge transfer process.<sup>16,17</sup> However, their potential applications are still restricted since they experience an inadequate rate capability and cycling performance due to their slow charge transfer kinetics and low electrical conductivity. Nevertheless, the compounds of transition metals with layered structures are fascinating because of their great potential for the fast ion diffusion that allows maximum insertion and extraction of electrolyte ions into the interlayer spaces of the electrode material.<sup>18</sup> The ultrathin layered crystals will endow the electrode material with several

Received: July 31, 2020

advantages such as a large surface area available for electrolyte interaction. The edges of layered sheets provide higher electrochemical activity than the planar surface to store more metal ions due to the intercalation, and these crystal structures are less fragile, providing high mechanical strength for flexible wearable devices.<sup>19</sup> Transition metal dichalcogenides (TMDs) exhibit a two-dimensional (2D) layered structure with strong covalent intralayer and weak interlayer van der Waals interactions which make them good hosts for the inclusion of electrolyte ions.<sup>20,21</sup> These ions are repeatedly inserted into the van der Waals gaps for the storage and delivery of charges through the adjacent layers. The incorporation of carbon and/or nitrogen atoms into the early transition metals forms another group of inorganic compounds (MXenes), which present layered formation with high electrical conductivity, hydrophilicity, and excellent mechanical strength.<sup>22</sup> These characteristics are associated with the covalent, ionic, and metallic bonds between the atoms in MXenes.<sup>23</sup> The covalent nature of interaction produces a low postintercalation volume expansion that brings excellent stability to the structures. Furthermore, excellent ionic properties and high electrical conductivity of the transition metal atoms are desirable for charge storage and delivery.<sup>24</sup> Besides these compounds, another class of electrode materials includes the transition metal oxides/hydroxides (TMOs/TMHs), which are considered superior due to their exceptional theoretical capacities (e.g., RuO<sub>2</sub>, ~1400–2200 F g<sup>-1</sup>; MnO<sub>2</sub>, 1370 F g<sup>-1</sup>), rapid reversible electron transfer, and their abundance in nature.<sup>25,26</sup> Oxides/hydroxides of transition metals can reveal surface redox reaction or intercalation dominated pseudocapacitance depending on their structure and charge storage behavior.<sup>27</sup> The morphology of TMOs and TMHs can be tailored through facile synthesis procedures which often require a relatively low temperature.<sup>28</sup> The morphology and size are important parameters to determine the diffusion kinetics and cyclability of the electrode materials. Bulk transition metal compounds suffer from intrinsic low electrical conductivity; however, their 2D structures provide a high surface area to demonstrate fast ion diffusion and high electrical conductivity. Besides, there are opportunities for further research aimed at the amalgamation of diverse capacitive materials to obtain hybrid systems, which produce an enhanced electrochemical performance owing to the synergistic effect established between active materials. The performance of MSCs depends not only on the attributes of active materials but also on the configuration and arrangement of microelectrodes.<sup>29</sup>

The morphology and size are important parameters to determine the diffusion kinetics and cyclability of the electrode materials.

Hence, there is a constellation of materials and composites with EDL or pseudocapacitance that are being developed to realize the high-performance MSCs. This Outlook highlights the latest advances of highly electroactive 2D TMDs, MXenes, and TMOs/TMHs in the assembly of MSCs with a planar configuration (Figure 1). The critical issues of structural aggregation and inherently low electrical conductivity associated with the conventional transition metal compounds

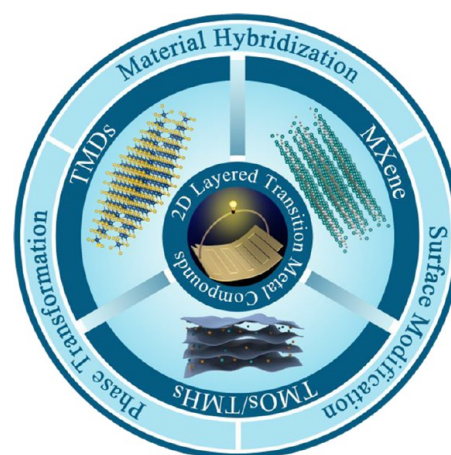


**Figure 1.** Schematic illustration of 2D electrode materials based on transition metals for the micro-supercapacitor.

hinder their wide-ranging applications. Herein, we presented impactful strategies to overcome these obstacles by structural engineering for tuning the crystal structure, porosity, and electrical conductivity of the metallic phase. Additionally, various coupling principles are elucidated to rationally integrate the composite hybrids and asymmetric configurations of electrodes to construct the MSCs with high electrochemical performance.

## 2. TRANSITION METAL DICHALCOGENIDES (TMDs)

TMDs represent a family of 2D layered inorganic materials with a generalized chemical notation MX<sub>2</sub>, where M denotes a transition metal atom (Mo, W, V, etc.), and X is a chalcogen atom (S, Se, or Te). The transition metal atoms are covalently intercalated between two chalcogen layers, so their crystal constitutes a layered structure with weak interlayer van der Waals forces.<sup>30</sup> Recently, owing to their attractive physicochemical properties such as high surface area, electrochemical activity, mechanical permanency, excellent processability, and low cost, these materials have triggered wide research for utilization in the fields of energy storage, hydrogen evolution electrocatalysis, solar systems, sensors, biotechnology, and nanoelectronics.<sup>31,32</sup> Their heterostructures could convert the indirect band gap to a direct band gap, which is critical for electrocatalytic conversion, electrochemical energy storage, and applications in other electronics. Regarding energy storage, the reduced dimension of the atomically thin MX<sub>2</sub> layer offers the electrolyte a maximized contact with the active electrode for Faradaic and non-Faradaic interactions, and the interlayer spaces act as excellent hosts for swift ion diffusion ensuring the higher utilization of material for developing high-performance electrodes.<sup>33</sup> Considering MoS<sub>2</sub> as a prominent candidate of TMD species, Cao et al. demonstrated a MSC based on 2D MoS<sub>2</sub> film, where microelectrodes were prepared by the spray painting of a hydrothermally prepared substance, followed by laser cutting.<sup>34</sup> The structured nanosheets expedite the approach of aqueous electrolyte ions to the electrode, and the cell exhibited an areal specific capacitance of 8 mF cm<sup>-2</sup> but showed insufficient cycling performance due to self-restacking of nanosheets. Later, another perspective was given to reveal that exfoliated few-layered MoS<sub>2</sub> exhibits higher electrochemical activity than the bulk material, and in that particular study, MoS<sub>2</sub> flakes showed a capacitance of 2.4 mF cm<sup>-2</sup>, superior to the bulk counterpart (~0.5 mF cm<sup>-2</sup>).<sup>35</sup> The

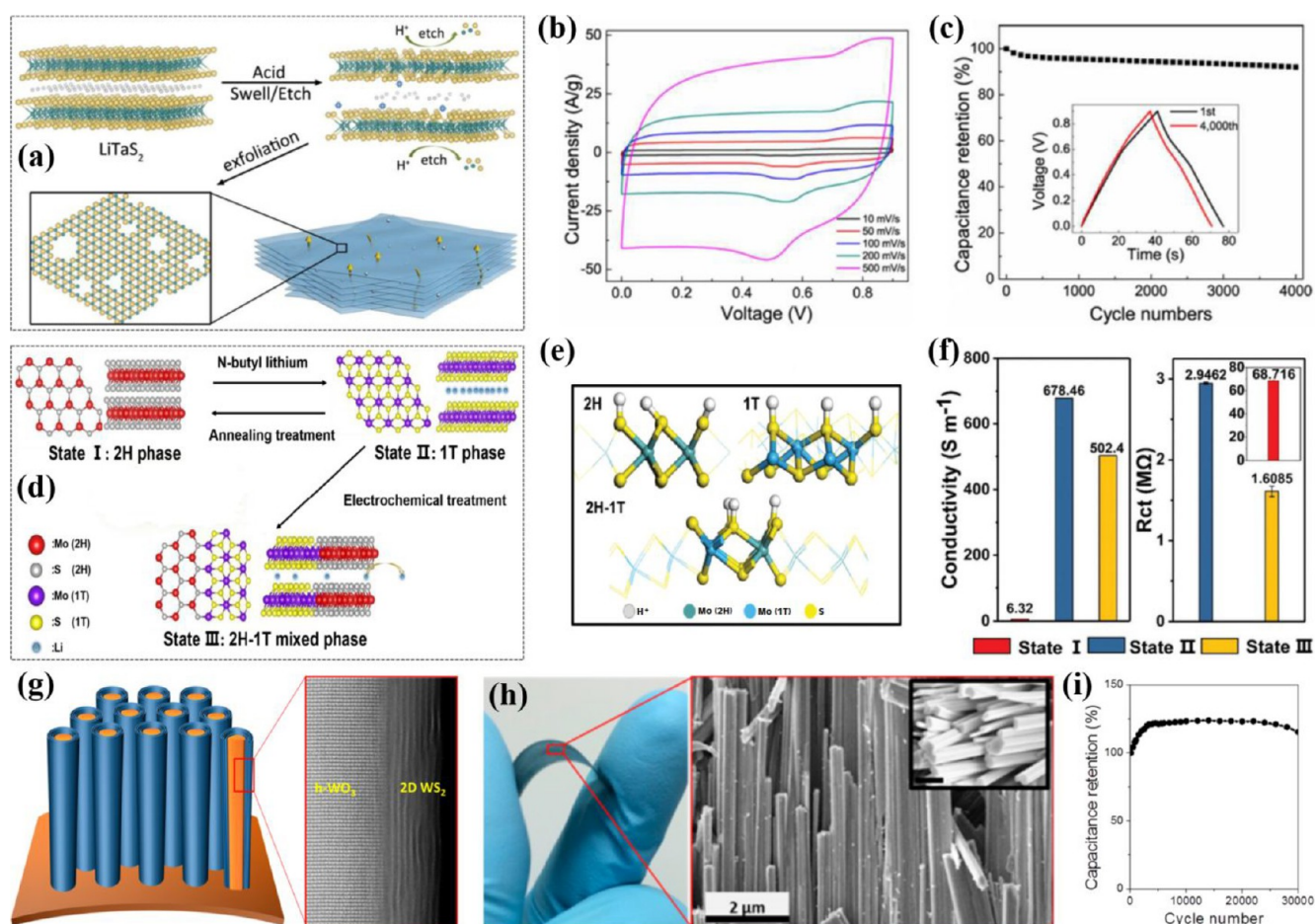


**Figure 2.** (a) Schematic illustration of acid-assisted etching and exfoliation to obtain  $TaS_2$  monolayers for the fabrication of MSC.<sup>39</sup> (b) CV curves at different scan rates and (c) cycling stability of the MSP- $TaS_2$ -based MSC at a current density of  $2\ A\ g^{-1}$ ; the inset is the GCD curves at the 1st and 4000th cycle. Schematic diagram of (d) the phase transition from state I to state III and (e) simulation of proton adsorption in the 2H, 1T, and mixed 2H-1T phases of  $MoS_2$ .<sup>41</sup> (f) Specific conductivity of three states and their corresponding  $R_{ct}$  values. (g) Scheme to visualize the one-body array of core/shell nanowires (left), and corresponding ADF-STEM image of  $WO_3/WS_2$  core/shell nanowire (right).<sup>47</sup> (h) Optical image under mechanical bending (left), and corresponding SEM image (right) of densely aligned core/shell nanowires; the inset shows their faceted surface. (i) Cycling performance at a scan rate of  $100\ mV\ s^{-1}$ . Reprinted with permission from refs 39, 41, and 47. Copyright 2018 American Chemical Society, 2020 Royal Society of Chemistry, 2016 American Chemical Society.

exfoliated structures still showed the problem of aggregation and restacking, reducing the performance, so their crystal structures are further modified. The later sections describe the significant developments in the utilization of 2D TMDs.

**2.1. 2D Metallic TMDs.** The phase engineering of chemically exfoliated sheets of metallic TMDs shows enhanced electrochemical behavior by allowing high intercalation of electrolyte ions. Research reveals that the metallic 1T (octahedral) phase of TMDs exhibits a higher electrochemical performance due to the enhanced electrical conductivity relative to the semiconducting 2H (trigonal prismatic) phase.<sup>36</sup> In this regard, earlier research employed chemical exfoliation to achieve highly concentrated metallic 1T phase  $MoS_2$  films.<sup>37</sup> The nanosheets showed the capability of efficient intercalation of H, Li, K, and Na cations so that the thin-film electrode delivered a specific capacitance ranging from  $400$  to  $700\ F\ cm^{-3}$  in various electrolytes. The high performance was attributed to the intrinsic hydrophilic property, electrical conductivity, and ability of exfoliated nanosheets to efficiently intercalate the electrolyte ions. It is anticipated that achieving the 1T metallic phase of various other TMDs through exfoliation would also show a progressive

electrochemical response. On this subject, another research effort which was published later demonstrated the electrochemical activity and stability of highly conductive metallic 1T- $WS_2$  nanoribbons.<sup>38</sup> The prepared electrodes exhibited a capacitance of  $2.81\ mF\ cm^{-2}$ , several factors higher than that of the semiconducting 2H- $WS_2$  electrode. The improved electrical conductivity and extended spaces for intercalation between the consecutive layers revealed the potential of 2D metallic TMDs for power applications. Wu et al. proposed one-step acid-assisted exfoliation for the synthesis and surface modification of a large monolayer of  $TaS_2$  (Figure 2a).<sup>39</sup> Acid treatment of  $LiTaS_2$  yielded the metallic sub-nanopore  $TaS_2$  (MSP- $TaS_2$ ) with simultaneously exploiting the etching property of the hydrogen ion ( $H^+$ ) for porosity engineering to obtain a pore size of  $\sim 0.95\ nm$ , which was optimized with the size of electrolyte ions to provide fast ion transport kinetics. The interdigital MSC based on MSP- $TaS_2$  microelectrodes delivered a specific capacitance of  $508\ F\ cm^{-3}$  and an energy density of  $58.5\ Wh\ L^{-1}$ . The quasirectangular cyclic voltammetry (CV) curves showed the dominant EDL capacitive behavior in the voltage range  $0$ – $0.9\ V$ , which corroborates the effective electrolyte ion permeation through

the MSP-TaS<sub>2</sub> film (Figure 2b). Furthermore, the MSC showed improved cyclability, and 92% of the original capacitance was retained after 4000 cycles (Figure 2c). In another report, metallic 2D 1T-VSe<sub>2</sub> exfoliated nanosheets were prepared by employing a facile ambient pressure chemical vapor deposition (AP-CVD) technique.<sup>40</sup> A flexible in-plane supercapacitor was fabricated with high mechanical strength, demonstrating a stable performance even after 10 000 bending cycles. The prepared device presented dominant EDL behavior with a capacitance of 4.17 mF cm<sup>-2</sup> in PVA/KNO<sub>3</sub> gel electrolyte. 1T-MoS<sub>2</sub> has also been extensively employed in energy storage due to its plentiful active sites and virtuous conductivity, though it is thermodynamically unstable owing to the slanted crystal structure. Recently, the Mai research group monitored a mixed 2H-1T phase of MoS<sub>2</sub>, which possesses optimal performance and high stability.<sup>41</sup> Initially, 2H-MoS<sub>2</sub> was lithiated to obtain a 1T-MoS<sub>2</sub> nanosheet micro-/nanodevice, followed by the electrochemical treatment for transition to the stable 2H-1T mixed phase of MoS<sub>2</sub> (Figure 2d). The 2H-1T mixed phase retained a lower adsorption energy at the boundary, allowing the protons to easily combine at the boundary instead of adsorbing on the surface of S atoms in 2H and 1T phases (Figure 2e). The electronegativities of Mo and S atoms are higher at the boundary in the 2H-1T phase as compared to the 2H and 1T phases. Although the I–V measurements showed the higher electrical conductivity of the 1T phase because of it being pure metallic in nature, practically, the 2H-1T mixed phase had the smallest specific value of  $R_{ct}$  (Figure 2f). The smallest impedance of the 2H-1T phase revealed by EIS showed the best charge transfer rate in the mixed phase. Since various exfoliated metallic nanosheets exhibit a hydrophobic nature, they are still prone to aggregation, which is further annihilated by the growth and integration of other nanostructures.

The phase engineering of chemically exfoliated sheets of metallic TMDs shows enhanced electrochemical behavior by allowing high intercalation of electrolyte ions.

**2.2. Hybrid Composites of 2D TMDs.** Usually, the pure TMDs have 3 phase structures: 1T phase with fine conductivity, 2H with poor conductivity, and 3R phase with almost insulation.<sup>42</sup> The electrochemical performance of pristine TMDs is considerably low owing to the intrinsic low conductivity and the property of restacking.<sup>43</sup> The hybridization of TMDs with other conductive materials influences the physicochemical properties to realize better exploitation of charge storage and to show improved cycling stability through mechanical reinforcement and better rate capability of the conductive hybrid.<sup>44,45</sup> Wang et al. composited VSe<sub>2</sub> with carbon nanotubes (VSe<sub>2</sub>/CNT) through a one-step CVD method to fabricate a solid-state flexible in-plane supercapacitor.<sup>46</sup> The authors reported that VSe<sub>2</sub> nanosheets effectively exposed the surface for charge storage, and the CNT had a high conductivity and mechanical strength. Only 7% of capacitance was reduced after 10 000 charge–discharge cycles, and 91% of the original capacitance was retained after bending the device up to an angle of 40°. A distinct study by

Jung and co-workers reported a flexible core/shell supercapacitor based on a 1D single-crystalline tungsten trioxide (WO<sub>3</sub>) core seamlessly integrated with a 2D WS<sub>2</sub> layered shell.<sup>47</sup> The interface was self-assembled without any binder to form a one-body architecture (Figure 2g). The electrode design and material presented multifold advantages such as densely aligned nanowires providing a large surface area for ion adsorption/intercalation, sub-nanometer gaps of the WS<sub>2</sub> layer facilitating electrolyte ion insertion, and the conductive core having efficiently drawn out the charges (Figure 2h). This hybrid formation confirmed the excellent synergistic behavior of WO<sub>3</sub>/WS<sub>2</sub> core/shell nanowires through performing the electrochemical performance measurements using a three-electrode setup. The quasymmetrical CV loops corroborated the dominant EDL capacitance over the Faradaic behavior in the voltage range from –0.3 to 0.5 V. The slight deviation of CV curves from the ideal rectangular shape indicated some degree of redox reaction taking place by the intercalation of electrolyte ions, and the increasing skewness from the symmetrical curve at scan rates beyond 200 mV s<sup>-1</sup> is ascribed to the enhanced accumulation of electrolyte ions on the electrode surface. The initial capacitance of the nanowire-based supercapacitor was calculated to be 47.5 mF cm<sup>-2</sup> at 5 mV s<sup>-1</sup>; however, the capacitance increased to 74.25 mF cm<sup>-2</sup> at the same scan rate after 2500 cycles. During the cycling, it was observed that the capacitance continued to increase up to 2500 cycles because the WS<sub>2</sub> shell became electrochemically more active as the exposure of layers to electrolyte increased with cycles. The device showed an exceptional cycling performance with no decline in capacitance even after 30 000 charge–discharge cycles (Figure 2i). After 30 000 cycles, material characterizations revealed the exceptional structural and chemical stability of WO<sub>3</sub>/WS<sub>2</sub> nanowires. The practicability of the reported supercapacitor was determined by the maximum energy density of 0.06 W h cm<sup>-3</sup>.

Another strategy removed the barriers in the progress of TMDs by preparing a composite of a MoS<sub>2</sub> nanosheet-wrapped CoS<sub>2</sub> nanotube array via a facile hydrothermal reaction route.<sup>48</sup> This collaboration endowed high capacitance where the conductive channels of CoS<sub>2</sub> nanotubes offered large expandable spaces for volume change to prevent the aggregation, and the MoS<sub>2</sub> nanosheets provided more active sites for effective electrolyte accessibility. It is evident that the hybridization with a conductive basis reveals the approach for rational design and synthesis of diverse TMD electrodes. Li et al. demonstrated the development of an interpenetrated nanowire network in which Ag nanowires provided a highly conductive basis for collection and transport of charge carriers, and 2D metallic 1T phase MoS<sub>2</sub> nanosheets were employed as an ultrathin hydrophilic capacitive covering (Figure 3a).<sup>49</sup> It was elucidated that the electrolyte protons inserted into the interlayer spacing of clad MoS<sub>2</sub> to combine with electrons and produced a redox mechanism (Figure 3b). Based on the transparent films of clad AgNWs-MoS<sub>2</sub>, a highly flexible MSC was fabricated (Figure 3c), which delivered an auspicious electrochemical performance and high rate capability with a specific capacitance of 27.6 mF cm<sup>-2</sup> at 0.2 V s<sup>-1</sup>, reduced to 16.9 mF cm<sup>-2</sup> at a high scan rate of 3 V s<sup>-1</sup>. The MSC exhibited a specific energy density of 2.45 μW h cm<sup>-2</sup> and a corresponding power density of 1.47 mW cm<sup>-2</sup>. Furthermore, the MSC performed well during stability measurements by losing only 3.6% of the initial capacitance after 10 000 cycles (Figure 3d). The mechanical strength and bendability of the

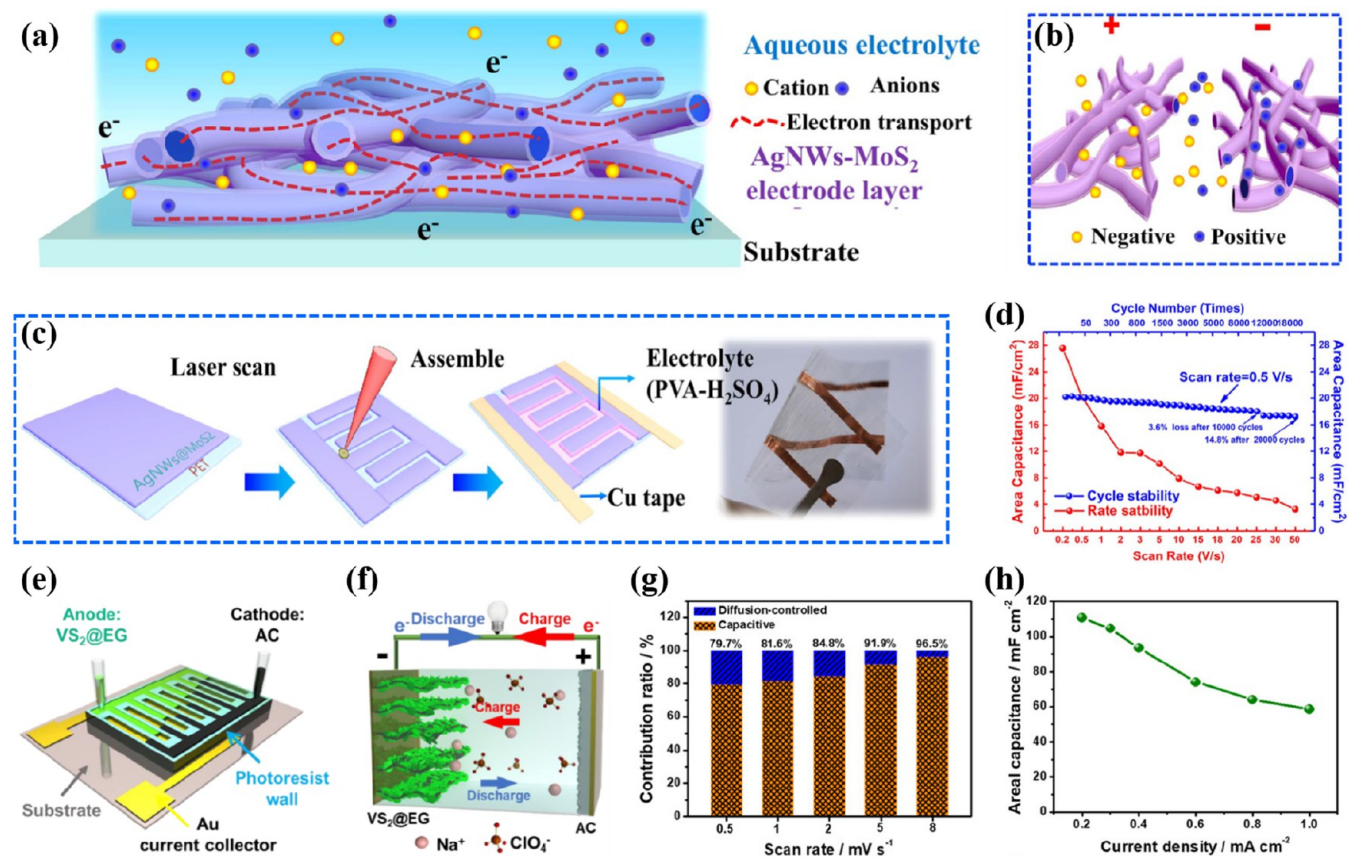


**Figure 3.** Schematic representation of (a) AgNWs-MoS<sub>2</sub> illustrating the electron transport, (b) ion diffusion in the microelectrodes during charging, and (c) laser-patterning of a flexible, transparent MSC.<sup>49</sup> (d) Cycling stability up to 20 000 cycles at 0.5 V s<sup>-1</sup> and rate capability at different scan rates. (e) Schematic illustration of transferring active materials into the microchannel for the asymmetric hybrid configuration of VS<sub>2</sub>@EG/AC-MSC.<sup>53</sup> (f) Working mechanism of MSC during charging and discharging. (g) Contribution ratio of capacitive and diffusion-controlled behavior at different scan rates. (h) Specific areal capacitance as a function of current density. Reprinted with permission from refs 49 and 53. Copyright 2019 Elsevier, 2019 Wiley-VCH.

device were tested by bending it to an angle of 180° 100 times, and the device showed a slight degradation of 1.4% in capacitance as compared with the normal state.

**2.3. Asymmetric Hybrid 2D TMD-MSCs.** To enhance the energy capabilities of MSCs, the asymmetric assembly is an effective strategy to extend the working voltage range through the combination of dissimilar microelectrodes.<sup>50,51</sup> For example, Moosavifard et al. obtained interdigital micropatterns of laser scribed graphene (LSG) onto the flexible PET substrate followed by the selective electrodeposition of CoNi<sub>2</sub>S<sub>4</sub> to construct a flexible MSC.<sup>52</sup> Here, LSC/CoNi<sub>2</sub>S<sub>4</sub> and LCG worked as the positive and negative interdigital microelectrodes, respectively, with GO as the separator and PVA/KOH gel electrolyte to formulate a hybrid all-solid-state flexible MSC. The device exhibited EDL and pseudocapacitive mechanisms simultaneously in a potential range of up to 1.7 V, which is the characteristic of a hybrid system. The stack capacitance was evaluated in correspondence to the deposition cycles, and a maximum capacitance of 122.4 F cm<sup>-3</sup> was obtained with 15 deposition cycles. The MSC showed an outstanding cycling performance, retaining 93.9% of the original capacitance after 10 000 charge–discharge cycles at 15 A cm<sup>-3</sup>, and the CoNi<sub>2</sub>S<sub>4</sub> nanosheets remained stable even after the cycling. Here, graphene was considered as a “superhighway” for fast electron transport, and CoNi<sub>2</sub>S<sub>4</sub> nanosheets provided a large surface area for the redox activity

to enhance the overall performance. The MSC showed excellent flexibility up to a bending angle of 180° and delivered an energy density of 49 W h L<sup>-1</sup>. Another work by Feng’s group described the construction of a new type of hybrid asymmetric MSC by formulating hierarchical VS<sub>2</sub> nanosheets grown on the electrochemically exfoliated graphene (EG).<sup>53</sup> VS<sub>2</sub>@EG served as the negative electrode; activated carbon (AC) was employed to fabricate the positive electrode, and the nonaqueous NaClO<sub>4</sub> dispersion was used as the electrolyte (Figure 3e). The hierarchical nanostructures of VS<sub>2</sub>@EG exposed the surface for rapid insertion/extraction of ions, and the AC enabled high adsorption/desorption resulting in a high rate capability and reversibility during charge–discharge (Figure 3f). The balanced mass distribution of electrode materials was attained to demonstrate a high-efficiency hybrid MSC, which worked within the large voltage range 0.01–3.5 V. The hybrid MSC delivered a specific capacitance of 110.7 mF cm<sup>-2</sup> at 0.2 mA cm<sup>-2</sup> and maximum energy and power densities of 188.3 μW h cm<sup>-2</sup> and 5.9 mW cm<sup>-2</sup>, respectively. Moreover, the device showed no noticeable capacitance degradation after charging and discharging 5000 times; rather, there was an increase in capacitance that could be attributed to wettability and good penetration of the electrolyte after several cycles. The synergistic effect was due to the dissimilar capacitive mechanisms of the VS<sub>2</sub>@EG anode and AC cathode. The ratio of the pseudocapacitive

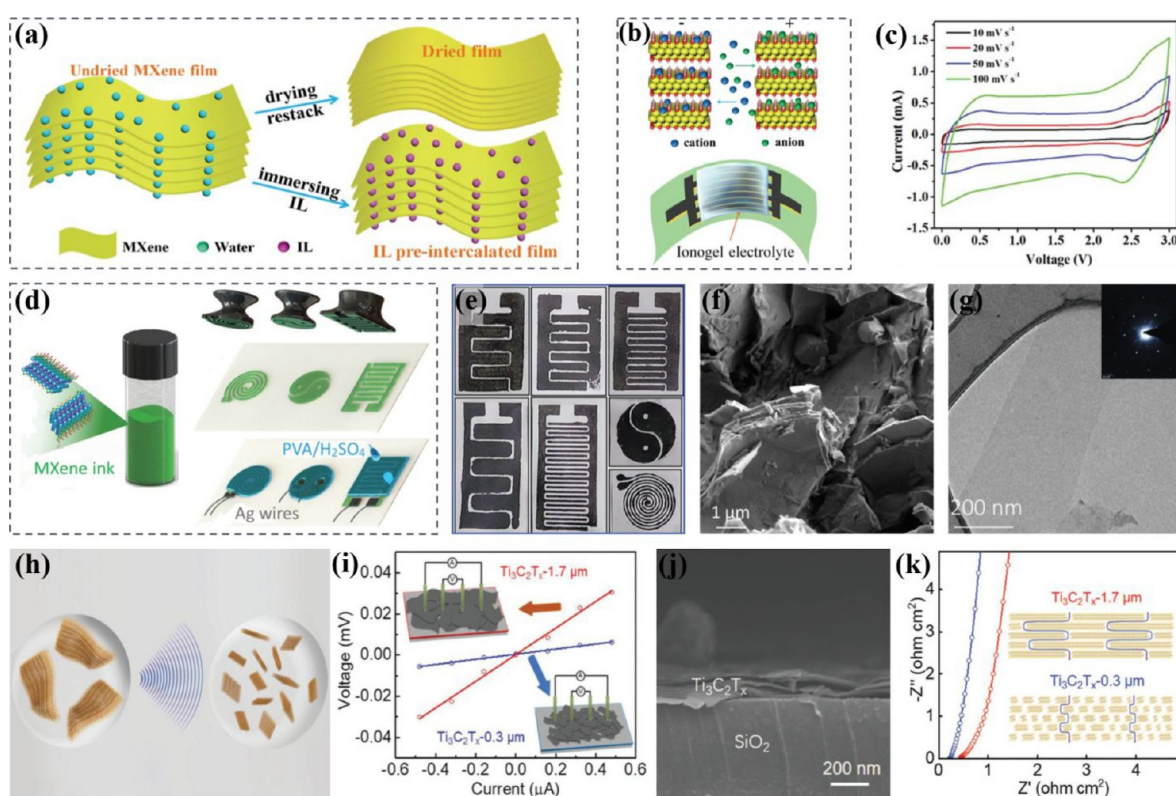


**Figure 4.** Schematic diagram of the (a) production of IL preintercalated and dried MXene electrode films and (b) preintercalated MXene MSC with ionogel electrolyte, and parallel ion transfer between the films.<sup>65</sup> (c) CV curves (from 10 to 100 mV s<sup>-1</sup>) of MSC. (d) Representation of Ti<sub>3</sub>C<sub>2</sub>T<sub>x</sub> nanosheet ink-based MSCs using the stamping approach.<sup>66</sup> (e) Digital photo of stamped MSCs with different designs. (f) SEM image of multilayered Ti<sub>3</sub>C<sub>2</sub>T<sub>x</sub> flakes. (g) TEM image of dried Ti<sub>3</sub>C<sub>2</sub>T<sub>x</sub> flakes; the inset is the selected area electron diffraction (SAED) pattern. (h) Schematic for tuning MXene flake size by sonication.<sup>67</sup> (i) *I*–*V* characteristics of spray-coated MXene films of different flake sizes; the inset shows the schematic of the four-point probe conductivity measurement. (j) SEM image of a cross-section showing spray-coated Ti<sub>3</sub>C<sub>2</sub>T<sub>x</sub> thin films. (k) Nyquist plot and schematic illustration of typical ion diffusion paths of MXene films with different flake sizes. Reprinted with permission from refs 65, 66, and 67. Copyright 2019 Royal Society of Chemistry, 2018 and 2019 Wiley-VCH.

contribution by VS<sub>2</sub>@EG kept increasing at higher scan rates owing to the exposed active surface sites for the rapid Na<sup>+</sup> insertion/extraction, and the MSC presented a high rate capability due to the hierarchical porous structure (Figure 3g,h). Other than typical graphene, various carbon-free TM chalcogenides (e.g., CuSe) revealed a better affinity with Au current collectors to provide a conductive scaffold. For instance, transition metal oxyhydroxides (MOOH: FeOOH and MnOOH) were alternatively deposited onto vertically oriented CuSe nanosheets with interspaces of 2–3 μm for better utilization of MOOH.<sup>54</sup> The asymmetric MSC exhibited a specific capacitance of 20.47 mF cm<sup>-2</sup>, excellent cycle performance (95% remained after 32 000 cycles), a high energy density of 16 mW h cm<sup>-3</sup>, and a power density of 1299.4 mW cm<sup>-3</sup>. Forgoing research spurred the rationality of asymmetric assembly design, which facilitated MSCs to operate steadily in an extended voltage window for the enhancement of energy density.

### 3. TRANSITION METAL CARBIDES AND/OR NITRIDES (MXENES)

MXenes are 2D inorganic materials based on transition metal carbides and/or nitrides and are emerging as high-performance materials for applications in Li/Na-ion energy-storage systems, supercapacitors, and water purification. The common notation of MXenes is M<sub>n+1</sub>X<sub>n</sub>T<sub>x</sub> in which M represents the transition metals (Ti, Cr, Mo, V, Nb, Zr, etc.) and X carbon or nitrogen;

*n* is an integer from 1 to 3, and T<sub>x</sub> stands for the surface termination group like hydroxyl, oxygen, or fluorine. The surface termination groups reduce the hydrophilicity and significantly influence their electrical properties.<sup>55,56</sup> MXenes are obtained by selective etching of the “A” layer from the MAX phase and added “ene” to the end for revealing its 2D nature. Since their discovery, MXenes have received tremendous attention in the field of energy storage due to their exceptional structures. For example, they have efficient electron transport owing to their highly conductive inner transition metal carbide layer and large active sites for fast surface redox reactions comparable with transition metal oxides. Out of more than 20 reported MXenes, titanium carbide (Ti<sub>3</sub>C<sub>2</sub>) is widely explored for applications in MSCs because of its high electrical conductivity (6.76 × 10<sup>3</sup> S cm<sup>-1</sup>), large specific capacitance (1500 F cm<sup>-3</sup>), and excellent rate performance (10 V s<sup>-1</sup>) in acidic electrolyte.<sup>57–59</sup> In addition to the high specific capacitance, MXenes possess a high mechanical stability due to their layered nature and are hence favorable for MSCs specifically.<sup>60</sup> Different electrolyte cations, for instance, Li<sup>+</sup>, K<sup>+</sup>, Na<sup>+</sup>, NH<sub>4</sub><sup>+</sup>, Al<sup>3+</sup>, etc., can intercalate in the MXene layers during the electrochemical process, which makes them promising candidates for supercapacitors and multivalent ionic electrolyte batteries.<sup>61</sup> Contrary to charge storage onto/into the electrode surface by adsorption of electrolyte ions, MXenes store charge through fast reversible redox reactions, offering high volumetric capacitance at a high

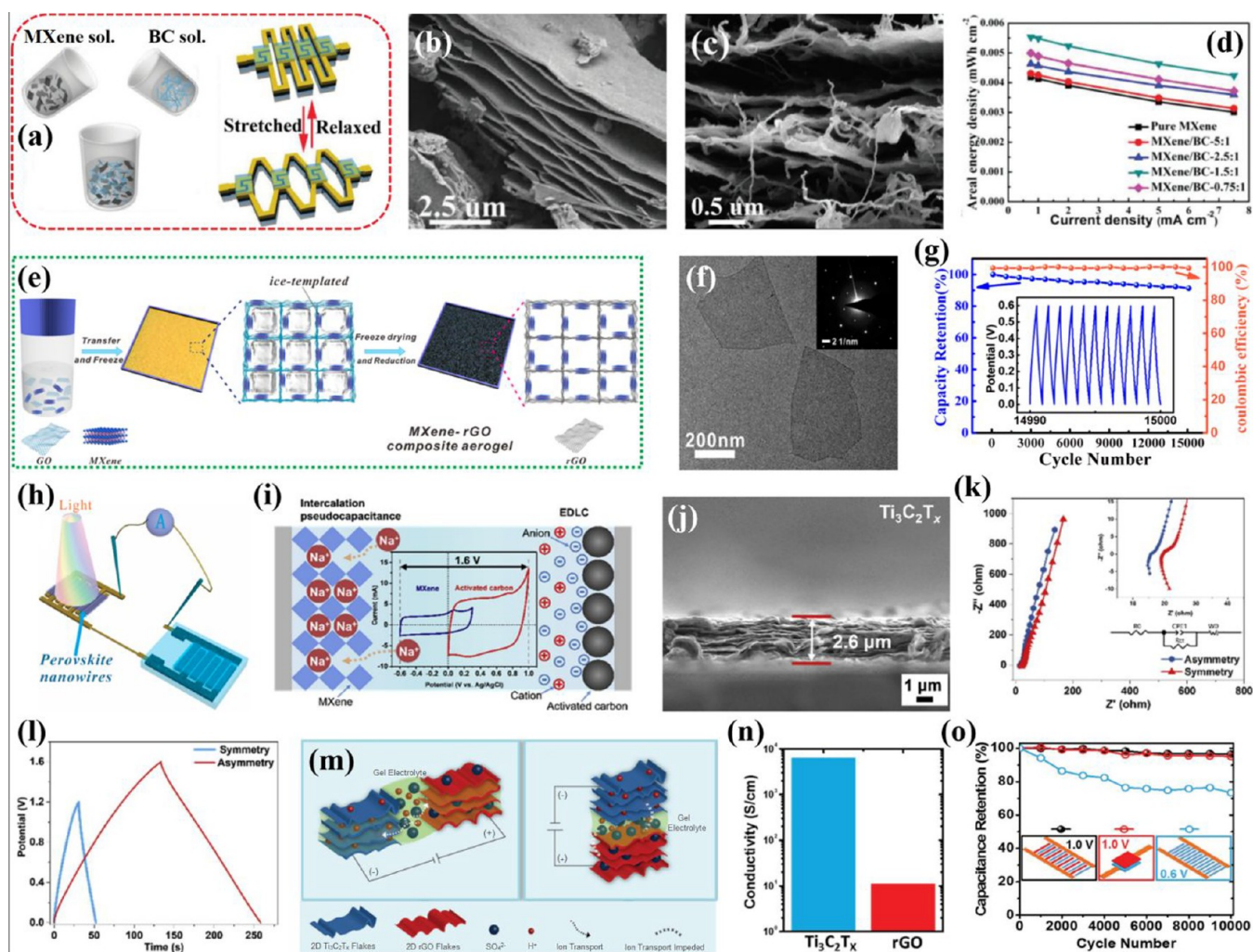


**Figure 5.** (a) Schematic diagram of the MXene/BC solution, and MSCs in stretched and relaxed states.<sup>73</sup> Representative SEM images of (b) etched multilayered MXene sheets and (c) MXene/BC composite showing BC fibers inserted between the MXene layers. (d) Areal energy densities of MSCs based on pure MXene and MXene/BC composites prepared with different mass ratios. (e) Schematic of the protocols for preparing MXene-rGO composite aerogel.<sup>76</sup> (f) TEM image of two MXene nanoflakes; inset is the corresponding SAED pattern. (g) Capacitance retention of the fabricated MSC when cycled at  $2 \text{ mA cm}^{-2}$ ; inset is the GCD curve of the last 11 cycles. (h) Demonstration of MSCs operating a photodetector. (i) Schematic illustration of the charge storage mechanism of an asymmetric MSC; inset shows the CV curves of MXene and AC electrodes at a scan rate of  $10 \text{ mV s}^{-1}$ .<sup>77</sup> (j) Cross-sectional SEM image indicating the thickness of the  $\text{Ti}_3\text{C}_2\text{T}_x$ -based negative electrode. (k) Nyquist plots and the fitted equivalent circuit and (l) GCD curves of MXene-based symmetric and MXene/AC asymmetric MSCs. (m) Schematic demonstration of ion transport in interdigital and sandwich configurations of asymmetric MSCs based on 2D  $\text{Ti}_3\text{C}_2\text{T}_x$ /rGO flakes.<sup>78</sup> (n) Electrical conductivities of  $\text{Ti}_3\text{C}_2\text{T}_x$  and rGO films. (o) Stability of different AMSCs and a symmetric MSC bent at  $30^\circ$  during cycling at  $0.2 \text{ mA cm}^{-2}$ . Reprinted with permission from refs <sup>73</sup> and <sup>76–78</sup>. Copyright 2019 Wiley-VCH, 2019 American Chemical Society, 2020 Elsevier, 2018 Wiley-VCH.

charge/discharge rate with excellent electrical conductivity. Most of the MXene-based MSCs reported so far have displayed limited areal energy density ( $<10 \text{ mW h cm}^{-2}$ ) due to their small operating voltage range in aqueous electrolytes (0.6–1.0 V). Herein, we describe the latest substantial developments in the MXene-based MSCs.

**3.1. Pristine MXene-Based MSCs.** Ionogel is a specific quasi-solid-state electrolyte in which ionic liquids (ILs) are assimilated into the suitable polymer matrix during polycondensation, and their exceptional thermal stability empowers a wide operation temperature of MSCs, high working voltage window, and excellent cycling stability.<sup>62–64</sup> Zheng et al. reported the construction of a novel type of ionogel-based on-chip MSC by IL preintercalated MXene layers that operated in a high voltage and achieved a high volumetric energy density and extraordinary flexibility with segmental incorporation of

bipolar cells.<sup>65</sup> By using interdigital mask-assisted deposition of MXene onto the graphene support, the obtained microelectrodes realized a high electrical conductivity of  $2200 \text{ S cm}^{-1}$  and high stability for fast electron transfer without any polymer binder and conducting additives or the metal current collectors. Due to the IL preintercalation, the MXene-based film established a network of ion transportation with an extended interlayer spacing (1.45 nm), larger than those of undried (1.27 nm) and dried (1.09 nm) MXenes (Figure 4a,b). Furthermore, the MSC assembled with EMIMBF<sub>4</sub> electrolyte displayed a remarkable areal capacitance of  $140 \text{ F cm}^{-3}$ , a specific energy density of  $13.9 \mu\text{W h cm}^{-2}$  ( $43.7 \text{ mW h cm}^{-3}$ ), and exceptional flexibility with long-term cycling stability retaining ample capacitance by no loss up to 10 000 cycles. The enlarged pseudocapacitance of the electrochemically active MXene as shown by the CV curves in Figure 4c was

attributed to the expanded interlamellar spaces created by intercalated IL, which provided a large ion-accessible surface area and low ionic resistance, enabling interlayer nanochannels to accommodate more insertion/extraction of EMIM<sup>+</sup> cations. The arrangement of the highly conductive pseudocapacitive charge storage mechanism of MXenes with enhanced mechanical flexibility and squashed film design results in a favorable electrochemical performance. The Nicolosi research group developed an elegant and quick stamping technique to fabricate MSCs based on 2D Ti<sub>3</sub>C<sub>2</sub>T<sub>x</sub> nanosheets by slightly pressing the 3D printed stamps on paper substrates after coating with viscous MXene ink (Figure 4d).<sup>66</sup> The MXene ink constituted hexagonal structured Ti<sub>3</sub>C<sub>2</sub>T<sub>x</sub> nanosheets with an average lateral size of 1.2 ± 0.2 μm and thickness of ~1.5 nm. Taking advantage of the metallic conductivity of MXene nanosheets and homogeneous film morphology, the current-collector-free electrodes were designed with fast electron transport and high rate response (Figure 4e). Due to the favorable surface chemistry of the stamped MXene on paper, there was an enhanced accessibility of electrolyte ions deep inside the multilayered Ti<sub>3</sub>C<sub>2</sub>T<sub>x</sub> nanoflakes (Figure 4f,g). By applying the gel electrolyte and connecting Ag wire collectors, the constructed interdigital MSC revealed an areal capacitance of 61 mF cm<sup>-2</sup> at 25 μA cm<sup>-2</sup> and a retained capacitance of 50 mF cm<sup>-2</sup> at 800 μA cm<sup>-2</sup>.

The shortcoming of MXene-based MSCs fabricated by filtration or the stamping method is the control of interspaces between the electrode fingers to achieve a high-frequency response with low relaxation time constant ( $\tau_0$ ). Solution-processed pseudocapacitive materials usually display limited electrical conductivity resulting in a low charge transfer rate and, hence, are not suitable for AC-line filtering applications. The significant characteristics in the construction of AC-line filtering capacitors include a high surface area with optimal pore size to lower the electrolyte resistance, high ion/electron conducting layered materials with minimal interspace resistance, and strong ohmic contact between electrode materials and current collectors to lower the impedance. Jiang and coresearchers designed a solution-processable 2D Ti<sub>3</sub>C<sub>2</sub>T<sub>x</sub> nanosheet-based interdigital MSC by optimizing the flake size and device architecture resulting in a high-frequency response device comparable with an electrolytic capacitor.<sup>67</sup> The suspension of Ti<sub>3</sub>C<sub>2</sub>T<sub>x</sub> was ultrasonicated for 45 min by a tip sonicator (Figure 4h) to obtain smaller flake sizes (0.3 μm). For the construction of the MSC, standard photolithography and a lift-off process were employed, followed by the spray coating of the MXene. The Ti<sub>3</sub>C<sub>2</sub>T<sub>x</sub> dispersion was spray coated onto the hydrophilic gold current collectors to obtain a uniform distribution and robust adhesion of MXene flakes with the metal surface. The interdigital MXene MSC was obtained after applying PVA/H<sub>3</sub>PO<sub>4</sub> gel electrolyte. The relationship of flake size and electrical conductivity of the MXene was observed by a four-probe method, and it was found that Ti<sub>3</sub>C<sub>2</sub>T<sub>x</sub> film with a smaller flake size (0.3 μm) displayed less electrical conductivity (900 S cm<sup>-1</sup>) compared with the larger flake size (1.7 μm) with an electrical conductivity of 4500 S cm<sup>-1</sup> (Figure 4i). Owing to the strong adhesion of Ti<sub>3</sub>C<sub>2</sub>T<sub>x</sub> sheets with metal collectors, the active material did not peel off even after bath sonication during the lift-off procedure (Figure 4j). The feasibility of the wafer-scale MXene-based MSC was tested, which displayed a specific capacitance of 30 F cm<sup>-3</sup>, a high rate performance up to 300 V s<sup>-1</sup>, and a relaxation time

constant of 0.45 ms which was shorter than conventional capacitors. Consequently, the device showed the filtering capability of 120 Hz ripples generated by an AC power line at 60 Hz. Interestingly, even though the electrical conductivity of Ti<sub>3</sub>C<sub>2</sub>T<sub>x</sub>-0.3 μm is low, it showed lower equivalent series resistance (ESR) (0.2 Ω cm<sup>2</sup>) than that of the Ti<sub>3</sub>C<sub>2</sub>T<sub>x</sub>-1.7 μm (0.5 Ω cm<sup>2</sup>), which indicated that ion access and dynamics are equally essential for high rate charge/discharge (Figure 4k).

**3.2. Composite Hybrids and Asymmetric MSCs.** An obstacle in large-scale applications of MXene-based electrodes is the restacking of nanosheets, which limits the intercalation of electrolyte ions resulting in the low areal specific capacitance of the constructed device. To prevent this issue, 1D carbonaceous materials (e.g., carbon nanotubes and carbon fibers) have been extensively used as interlayer spacers to prevent the restacking of MXene nanosheets for the ultimately enhanced performance of the composite electrode.<sup>68–72</sup> Nevertheless, the high production cost considerably limits their commercial applications on a large scale. Jiao et al. fabricated a high-performance stretchable, bendable, and twistable MSC based on fully delaminated few-layered 2D Ti<sub>3</sub>C<sub>2</sub>T<sub>x</sub> nanoflakes composited with 1D bacterial cellulose fibers (BC) through a solution-based paper making process followed by high-power laser cutting (Figure 5a).<sup>73</sup> Within the plane of this composite structure, the firmly stuffed MXene sheets offered profoundly productive electron transport pathways, whereas the BC fibers incredibly improved the mechanical stability of the composite by acting as an adhesive between the Ti<sub>3</sub>C<sub>2</sub>T<sub>x</sub> sheets, as displayed within the magnified cross-sectional image (Figure 5b,c). The fabricated MSC exhibited an areal capacitance of 111.5 mF cm<sup>-2</sup> without any apparent loss in capacitance during a tensile strain of 100% by bending and twisting. The MSC unit prepared by the composite showed a 132% enhancement in the areal energy performance compared to pure MXene (Figure 5d).

Another effective approach to prevent the agglomeration of MXene nanosheets is to employ graphene between MXene layers as a perfect spacer, thus improving the electrochemical properties of MXene.<sup>74</sup> However, due to the small size of MXene, the contact resistance between the slices eventually causes an increase in the internal resistance of the device.<sup>75</sup> A study by Yue and co-workers reported a simple method to construct a self-healing MSC by using MXene-rGO composite aerogel by a freeze-drying method followed by laser cutting (Figure 5e).<sup>76</sup> The MXene nanoflakes had a 2D lamellar structure with a lateral size of a few hundred nanometers (Figure 5f). When the blend arrangement of GO and MXene was solidified by freezing, the nanosheets were constrained to slowly adjust along the ice crystal boundary and ultimately cross-linked by the  $\pi$ - $\pi$  interaction to create a permeable network. The composite aerogel not only shared the high surface area of graphene and excellent conductivity of MXene but also prevented the self-restacking of the 2D lamellar structure and the oxidation of MXene. By using carboxylated polyurethane (PU) self-healable electrolyte, a flexible MSC was developed. The MXene-rGO aerogel-based MSC displayed a high areal specific capacitance of 34.6 mF cm<sup>-2</sup> at 1 mV s<sup>-1</sup>, with an excellent cycling performance and Coulombic efficiency after 15 000 cycles (Figure 5g). The practical application of the real product was shown by driving a photodetector of perovskite nanowires with a fully charged device (Figure 5h).

MSCs based on MXene present a high capacitive performance, rate capability, cyclability, and capability of AC filtering. However, due to its inception, the MXene-based electrodes still operate in a low positive potential, limiting the energy density for extensive practical applications. They suffer from excessive polarization at a voltage beyond the open circuit potential, which causes an increase in resistance and loss of adequacy.<sup>61</sup> Considering the foregoing issues, Xie et al. designed and fabricated a high-voltage asymmetric MSC by pairing  $\text{Ti}_3\text{C}_2\text{T}_x$  MXene as negative and activated carbon (AC) as positive electrodes via a cutting–spraying method.<sup>77</sup> The microelectrodes shared a broad working voltage of 1.6 V using the neutral PVA/ $\text{Na}_2\text{SO}_4$  gel electrolyte without partaking in any unacceptably excessive polarization (Figure 5i). The enhanced working potential intrinsically resulted in a boosted energy and power performance. Furthermore, the microelectrodes had an excellent transmission of electrolyte ions into the laminated morphology of MXene nanosheets with a thickness of 2.6  $\mu\text{m}$  (Figure 5j). The electrochemical performances of symmetric and asymmetric MSCs were compared, which showed the superiority of the asymmetric MSC (Figure 5k,l). Likewise, another research group applied the sequential spray coating of hydrophilic  $\text{Ti}_3\text{C}_2\text{T}_x$  MXene and rGO to develop a binder and current collector-free asymmetric MSC.<sup>78</sup> The MXene with high metallic conductivity facilitated the transfer of electrons, and the paired 2D layered materials enabled the fast ion diffusion (Figure 5m). The electrical conductivity of the  $\text{Ti}_3\text{C}_2\text{T}_x$  film was determined with a four-point probe system and found to be  $6400 \pm 120 \text{ S cm}^{-1}$  depending on the flake size and flake-to-flake contact resistance (Figure 5n). It was noted that the thin film of MXene (<100 nm) was semitransparent and, however, prone to undergo oxidation in air. That is why the thickness of the MXene layer needed to be optimized, or it would have required an inert atmosphere and nonaqueous electrolyte to provide stability. The asymmetric MSC showed a high electrochemical performance and the device exhibited a 97% capacitance retention after withstanding 10 000 charge–discharge cycles at various bending states up to  $90^\circ$  (Figure 5o).

MSCs based on MXene present a high capacitive performance, rate capability, cyclability, and capability of AC filtering.

#### 4. TRANSITION METAL OXIDES/HYDROXIDES (TMO/TMHS)

Among other pseudocapacitive 2D phases, layered TMOs/TMHS are becoming increasingly popular in micro-supercapacitors due to their high theoretical capacity, ample redox activity, chemically stable structure, and compatibility with electrolyte.<sup>79</sup> Typical bulk TMOs and TMHS possess an impeded rate capability due to their inherently low conductivity, slow charge diffusion, severe volume expansion, and aggregation,<sup>80</sup> while the 2D layered structures enhance the electrochemical performance and cyclability by shortening the ion flow path and offering a large surface area for electrochemical reaction.<sup>81</sup> Moreover, their planar 2D geometry is compatible with the planar devices, and the interlayer spaces

provide a certain degree of expansion to prevent their disintegration.<sup>82,83</sup> In this section, we describe various strategies that have been adopted to overcome the aforementioned challenges associated with the nature of typical TMOs/TMHS and realize the favorable features of layered structures in the applications for micro-supercapacitors.

**4.1. Pristine 2D TMOs/TMHS Electrodes.** Wu et al. demonstrated the design of a flexible MSC with 2D ultrathin  $\text{Ni}(\text{OH})_2$  nanoplates as the active electrode material.<sup>84</sup> The fabricated MSC displayed high capacitive properties with high bendability and cyclability by losing only 0.2% capacitance after 10 000 cycles. 2D TMH-based electrodes with a unique interconnected porous network, augmented nanopore array, and large surface area are vital for the construction of planar MSCs. Following this notion, Kurra employed a top-down photolithography protocol and bottom-up chemical bath deposition to obtain the MSC based on vertically oriented  $\text{Ni}(\text{OH})_2$  mesoporous nanoflakes with a thickness of 500 nm (Figure 6a).<sup>85</sup> Electrolyte ions rapidly diffused into the vertical nanoflakes and microelectrodes as the planar configuration showed no involvement of any separator (Figure 6b,c). The CV curves displayed two strong oxidation and reduction peaks, so it is evident that the  $\text{Ni}(\text{OH})_2$  lost the electron during the oxidation of  $\text{Ni}^{2+}$  to  $\text{Ni}^{3+}$ , and the process was rapidly reversible during the reduction (Figure 6d). The MSC showed redox activity even at higher scan rates due to the fast redox reaction, which corresponds to higher values of pseudocapacitance. The specific areal capacitance of the MSC determined from the discharge curve was  $16 \text{ mF cm}^{-2}$  with high energy and power performance. The planar MSCs exhibited fascinating virtues of thinness, fast charge/discharge competency, and long cyclability, making them prominent among microscale power supplies for integrated electronics. An outstanding MSC performance was achieved by full utilization of pseudocapacitive  $\text{MnO}_2$  with the assistance of nanoporous gold (NPG) to be current collectors and support for active TMO.<sup>86</sup> The fabricated MSC gave rise to more than 1 order of magnitude higher energy density compared to carbon/graphene-based MSCs through the rapid reversible redox reaction of thin-film  $\text{MnO}_2$  with proton incorporation and surface adsorption of  $\text{Li}^+$  cations from  $\text{LiCl}$  aqueous solution. Regardless of some effective presentations, pristine TMOs/TMHS electrodes display integrally low electrical conductivities, untimely ensuing low power density and rate performance.

**4.2. Composites of 2D TMOs/TMHS.** As stated above, the low conductivity and capacity decay of TMOs/TMHS due to the restacking of nanosheets after the long-term cycling process diminish their electrochemical properties.<sup>87</sup> Recently, defect engineering of 2D  $\text{MnO}_2$  nanosheets by atomic-level substitutional doping of transition metal cation ( $\text{Fe}^{3+}$ ,  $\text{Co}^{2+}$ , and  $\text{Ni}^{2+}$ ) has been proven to introduce new electronic states near the Fermi level, thus improving the natural electrical conductivity and the concentration of redox-active sites.<sup>88</sup> The influence of substitutional doping, in particular, the Fe doping, was observed in a symmetric MSC, which showed the superior electrochemical performance by delivering high energy and power densities. Gong et al. investigated electrochemically grown capacitive  $\text{Ni}(\text{OH})_2$  nanosheets on a conductive framework of predeposited  $\text{CuSe}$  nanosheets (Figure 6e).<sup>89</sup> It was elucidated that these particular  $\text{Ni}(\text{OH})_2$  NSs had a small lateral size (50 nm) and thickness (<10 nm), which enabled the high rate of ion intercalation compared to bulk

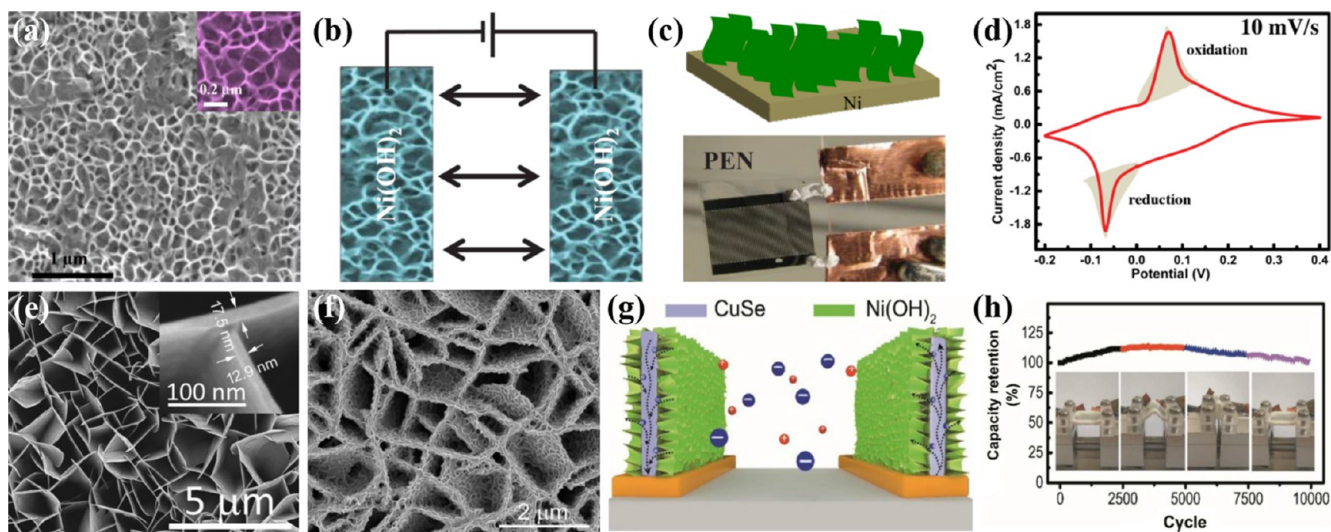


**Figure 6.** (a) Uniform vertically grown  $\text{Ni}(\text{OH})_2$  nanoflakes on substrate; inset shows the interconnected  $\text{Ni}(\text{OH})_2$  nanosheets.<sup>85</sup> Schematic illustration of (b) the in-plane configuration of microelectrodes and (c) the nucleation process of  $\text{Ni}(\text{OH})_2$  over the Ni surface; below is shown the photograph of MSC fabricated on the PEN substrate. (d) CV curve of  $\text{Ni}(\text{OH})_2$ -MSC in 1 M KOH electrolyte. SEM images of (e) the vertically oriented framework of interpenetrating CuSe NSs (inset shows the magnified image) and (f)  $\text{Ni}(\text{OH})_2$  nanosheets deposited onto the CuSe framework.<sup>89</sup> (g) Schematic illustrating the ion transport mechanism of the  $\text{CuSe}@\text{Ni}(\text{OH})_2$  NS-based hybrid in-plane MSC. (h) Cycling performance of the MSC under different bending states. Reprinted with permission from refs 85 and 89. Copyright 2015 Wiley-VCH, 2018 American Chemical Society.

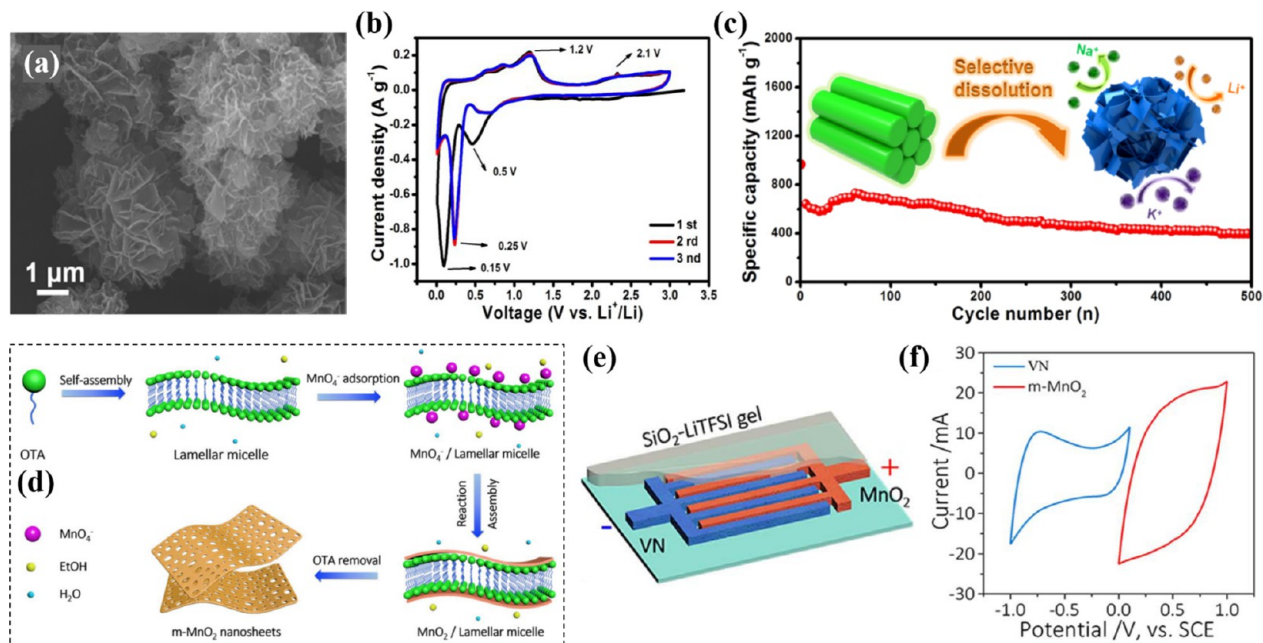


**Figure 7.** (a) FESEM image of ultrathin nanosheet-assembled hierarchical  $\text{Mn}_3\text{O}_4$ -G microflowers.<sup>91</sup> (b) CV curves of  $\text{Mn}_3\text{O}_4$  at  $0.1 \text{ mV s}^{-1}$ . (c) Cycling performance of  $\text{Mn}_3\text{O}_4$ -G at  $0.5 \text{ A g}^{-1}$ ; the inset shows the schematic diagram of selective dissolution to fabricate  $\text{Mn}_3\text{O}_4$ -G microflowers. Schematic shows the (d) synthesis of mesoporous  $\text{MnO}_2$  nanosheets and (e) configuration of asymmetric MSC.<sup>94</sup> (f) CV curves of  $\text{m-MnO}_2$  and VN NSs measured by the three-electrode setup. Reprinted with permission from refs 91 and 94. Copyright 2019 American Chemical Society, 2019 Elsevier.

structures (Figure 6f). This unique geometry overcame the poor conductivity and restacking of  $\text{Ni}(\text{OH})_2$  nanosheets; at the same time, the vertically aligned hybrid nanosheets provided enhanced pathways for ion transport into the electrodes (Figure 6g). The ESR of the MSC based on  $\text{CuSe}@\text{Ni}(\text{OH})_2$  was estimated to be  $92.2 \Omega$ , which was lower than pure  $\text{Ni}(\text{OH})_2$ -MSC ( $155.5 \Omega$ ). The MSC exhibited a specific capacitance of  $38.9 \text{ F cm}^{-3}$ , an energy density of  $5.4$

$\text{mW h cm}^{-3}$ , and a maximum power density of  $833.2 \text{ mW cm}^{-3}$ . A negligible drop in performance was observed without any loss in capacitance even after 10 000 cycles under varying bending states up to a  $180^\circ$  fold (Figure 6h). It was observed during the cyclic analysis that the device displayed an increase in the capacitance up to the initial 4000 cycles followed by a gradual decrease. The initial increase in capacitance was

attributed to the activation of redox-active species by exposure to the electrolyte with charge–discharge.

One of the challenges in MSCs is micronizing of active material on a small chip. The commonly used techniques such as electrochemical (EC) or electrophoretic (EP) deposition lead to material instability. Synthesizing 2D layered materials with patterning techniques is the ultimate solution. Birnessite manganese dioxide ( $\delta$ -MnO<sub>2</sub>) is an emerging electrode material for thin-film supercapacitors, possessing atomically thin layered structures, high theoretical capacity, environmental friendliness, and low cost. Recently, Wang et al. prepared highly concentrated ink of 2D  $\delta$ -MnO<sub>2</sub> nanosheets with a lateral size and thickness of 89 and 1 nm, respectively.<sup>90</sup>  $\delta$ -MnO<sub>2</sub> micropatterns were engineered on oxygen plasma-treated glass/polyimide substrate through inkjet printing without the undesired “coffee-ring” effect. By employing a PVA/LiCl gel electrolyte, a solid-state symmetric MSC was constructed displaying excellent capacitive, energy storage, and delivery performances with a capacitance loss of 12% after 3600 charge–discharge cycles. Mn<sub>3</sub>O<sub>4</sub> is another attractive anode material with the potential of high alkali-metal (Li/Na/K)-ion storage providing high capacity. Designing hierarchical structures is an effective approach to boost their charge storage capacity and cycling permanence by accommodating the volumetric changes in the spaces within substructures. Tang et al. utilized a selective dissolution strategy to produce hierarchical Mn<sub>3</sub>O<sub>4</sub>/graphene microflowers composed of ultrathin nanosheets with an excellent electrochemical performance and enhanced cycling stability.<sup>91</sup> The SEM image revealed the formulation of nanosheet-assembled Mn<sub>3</sub>O<sub>4</sub>-G microflowers with a size of 1–2  $\mu$ m (Figure 7a). The overlapping of the CV curve of the second and third cycles indicated the high reversibility of the Mn<sub>3</sub>O<sub>4</sub> electrodes (Figure 7b). Improved cycling stability was achieved by controlling the nanosheets’ interspace and designing hierarchical structures (Figure 7c).

Designing hierarchical structures is an effective approach to boost their charge storage capacity and cycling permanence by accommodating the volumetric changes in the spaces within substructures.

**4.3. 2D TMOs/TMHs-Based Asymmetric MSCs.** Asymmetric MSCs based on TMOs/TMHs draw further research interests because of their high energy capacity originating from the larger work function drop between dissimilar electrodes.<sup>92,93</sup> Qin et al. successfully synthesized a highly porous interconnected network of 2D mesoporous MnO<sub>2</sub> (m-MnO<sub>2</sub>) through the self-assembly strategy.<sup>94</sup> Ultrathin nanosheets were obtained with a thickness of 10 nm, mesopores of diameter ranging from 5 to 15 nm, and a surface area of 128 m<sup>2</sup> g<sup>-1</sup> (Figure 7d). The mesoporous network provided structural integrity during the cycling process, as these mesopores created enough void spaces to hold the increase in volume of nanosheets during charging and discharging. Mask-assisted layer-by-layer deposition was employed to obtain an asymmetric MSC device based on the positive electrode of as-prepared m-MnO<sub>2</sub> and negative electrode of vanadium

nitrate (VN) nanosheets (Figure 7e). The prepared mesoporous nanosheets and AMSC were tested in various other configurations, but the device tested with SiO<sub>2</sub>–LiTFSI gel electrolyte (VN/MnO<sub>2</sub>-AMSC-GE) yielded the best electrochemical performance. The microelectrodes with an optimized mass ratio of active materials kept a charge balance and operated in the wide potential range 0–2 V; besides, the pseudocapacitive behavior originated from the swift ion diffusion in the m-MnO<sub>2</sub> and VN nanosheets (Figure 7f). VN/MnO<sub>2</sub>-AMSC-GE presented a specific capacitance of 16.1 mF cm<sup>-2</sup>, a maximum energy density of 21.6 mW h cm<sup>-3</sup>, and a power density of 1539 mW cm<sup>-3</sup>. Furthermore, the AMSC retained 90% of the original capacitance after 5000 cycles, and 98% capacitance was retained after bending the device at an angle of 180°. Intercalating sodium ions Na<sup>+</sup> into layered TMOs could effectively increase the voltage window of the fabricated electrodes.<sup>95</sup> However, the growth of nanosheets on a common substrate is quite challenging. Recently, Zhang et al. successfully coupled hierarchical Na-MnO<sub>x</sub>@NCF/CNTF as the cathode and VN nanosheet arrays as the anode to assemble AMSCs which could operate in a broad voltage window of 2.4 V.<sup>96</sup> By applying Na<sub>2</sub>SO<sub>4</sub>/carboxymethyl (CMC) gel electrolyte, the constructed AMSC delivered a notable specific capacitance of 109.5 mF cm<sup>-2</sup> with an energy density of 87.62  $\mu$ W h cm<sup>-2</sup>. Besides, the AMSC exhibited greater mechanical stability with negligible decay after 3000 bending cycles. Combining the supercapacitive anode with a battery-like cathode into a single device produces a hybrid system with high performance. This was illustrated by constructing an all-solid-state flexible asymmetric MSC based on a vanadium nitrate (VN) nanosheet anode and redox-active Co(OH)<sub>2</sub> nanoflake cathode by employing the vacuum filtration technique.<sup>97</sup> In the first step, metal-free current collectors of chemically exfoliated graphene (EG) were fabricated on a nylon substrate through vacuum filtration followed by continuous deposition of 2D porous VN nanosheets as an anode and Co(OH)<sub>2</sub> as a cathode with 10% and 15% of EG as the conducting additive on either electrodes, respectively. By applying a thin film of PVA/KOH gel electrolyte, a specific capacitance of 21 mF cm<sup>-2</sup>, an energy density of 12.4 mW h cm<sup>-3</sup>, and a capacitance preservation of 84% over 10 000 cycles were achieved by the AMSC with high flexibility and facile integration strategy.

## 5. CONCLUSION AND OUTLOOK

The unique properties of electrochemically active 2D layered transition metal compounds endow a wide window of opportunities in achieving outstanding electrode materials for applications in micro-energy-storage systems. In particular, the exploration of MSCs is the platform of evolving thrust in research where these 2D inorganic materials show great potential toward coupling a highly energy-dense powering system to the planar, wearable, and flexible electronics. This Outlook focuses on recent experimental progress of 2D structural TMDs, MXenes, and TMOs/TMHs regarding their exceptional ultrathin geometry, large surface area, ample redox-active sites, tunable physicochemical properties, and outstanding flexibility. Along with the surface charge storage properties for high-level power, their variable oxidation states confer dominant energy density through the Faradaic charge storage mechanism of transition metal cations. The aforementioned properties are prerequisite for obtaining electrode materials with enhanced energy capacity, high rate capability,

and reliable cycling performance for MSCs. Nevertheless, some vital technical constraints remain to be resolved to achieve full exploitation of transition-metal-based 2D compounds as the active electrode materials for widespread practical applications.

The lamellar, porous structures form the basis of enhancing the active sites and specific surface area to achieve the efficient adsorption, intercalation, and ion transport for the enhancement of the electrochemical reaction. One-step exfoliation of bulk crystals has been proven to be an effective strategy to induce interlayer lattice expansion of exfoliated monolayer sheets to overcome the issue associated with the poor conductivity of TMOs/TMHs and TMDs; at the same time, the pore engineering through etching the basal plane produces uniform porous structures. Besides, the nanosheets prepared via soft chemical exfoliation have a degree of bendability that is desirable for a thin, mechanically robust, and flexible MSC. The alteration of the crystalline structure through the geometric shift of atoms yields an intriguing metallic 2D 1T phase which is hydrophilic and 107 times more conductive than the semiconducting 2H phase, while the nonterminated metallic MXene sheets intrinsically exhibit a high ionic/electronic mobility which renders them promising for the electrode material. Despite expanding the interlayer spacing, the bottleneck of 2D layered materials still lies in their tendency of inevitable aggregation due to interaction between charged nanosheets and electrolyte cations.

The interlayer spaces can be modulated by the incorporation of additional species, which stabilize the crystal structure of the host material, prevent the restacking of layers during the insertion/extraction of electrolyte ions, and enhance the electrochemical utilization of the entire layered structure. The hybridization of transition metal compounds through conductive additives produces high capacitance due to the increased electrical conductivity. Hierarchical integration of heterostructures would alleviate instability issues during the volume expansion and presents multifold advantages required for high electrochemical performance. The heterostructures with vertically aligned 2D nanosheets of smaller lateral size realize short diffusion pathways for electrolyte ions. Moreover, the direct contacts between nanosheets and conductive collectors fasten the electron transport through the interface in a coaxial direction. Therefore, the strongly coupled hybrid materials witness to overcome the various shortcomings associated with TMDs, MXenes, and TMOs/TMHs and produce synergistic effects more expedient than the individual counterparts. Nevertheless, the overall performance relies not only on the active materials but also on the construction of MSCs. Taking this into account, the asymmetric configuration is an effective strategy to utilize the extended working potential of two dissimilar microelectrodes for the enhancement of their energy density. Given the aforementioned challenges and achievements, it is anticipated that the surface chemistries and precise engineering of transition-metal-based 2D layered materials can pave the path for numerous opportunities to improve the intrinsic properties of electrode materials desired for the future endeavors in MSCs as the energy storage units for on-chip integrated systems.

## AUTHOR INFORMATION

### Corresponding Authors

**Liang He** – State Key Laboratory of Advanced Technology for Materials Synthesis and Processing, Wuhan University of

Technology, Wuhan 430070, China; [orcid.org/0000-0002-7402-9194](https://orcid.org/0000-0002-7402-9194); Email: [hel@whut.edu.cn](mailto:hel@whut.edu.cn)

**Yulai Han** – School of New Materials and New Energies, Shenzhen Technology University, Shenzhen 518118, China; Email: [hanyulai@sztu.edu.cn](mailto:hanyulai@sztu.edu.cn)

**Liqiang Mai** – State Key Laboratory of Advanced Technology for Materials Synthesis and Processing, Wuhan University of Technology, Wuhan 430070, China; Foshan Xianhu Laboratory of the Advanced Energy Science and Technology Guangdong Laboratory, Foshan 528200, China; [orcid.org/0000-0003-4259-7725](https://orcid.org/0000-0003-4259-7725); Email: [mlq518@whut.edu.cn](mailto:mlq518@whut.edu.cn)

## Authors

**Waqas Ali Haider** – State Key Laboratory of Advanced Technology for Materials Synthesis and Processing, Wuhan University of Technology, Wuhan 430070, China

**Muhammad Tahir** – State Key Laboratory of Advanced Technology for Materials Synthesis and Processing, Wuhan University of Technology, Wuhan 430070, China

**H. A. Mirza** – Department of Chemistry, York University, Toronto M3J 1P3, Ontario, Canada

**Ruiqi Zhu** – State Key Laboratory of Advanced Technology for Materials Synthesis and Processing, Wuhan University of Technology, Wuhan 430070, China

Complete contact information is available at:  
<https://pubs.acs.org/10.1021/acscentsci.0c01022>

## Notes

The authors declare no competing financial interest.

## ACKNOWLEDGMENTS

This work was supported by Foshan Xianhu Laboratory of the Advanced Energy Science and Technology Guangdong (XHT2020-003), the State Key Laboratory of Advanced Technology for Materials Synthesis and Processing (WUT:2019-KF-5, 2019-KF-2), the National Natural Science Foundation of China (51521001), the National Key Research and Development Program of China (2016YFA0202603), the Program of Introducing Talents of Discipline to Universities (B17034), the Shenzhen Science and Technology Innovation Free Exploration Project (JCYJ20170818140127741), and Natural Science Foundation of Top Talent of SZTU (2019010801009).

## REFERENCES

- (1) Li, H.; Liang, J. Recent Development of Printed Micro-Supercapacitors: Printable Materials, Printing Technologies, and Perspectives. *Adv. Mater.* **2020**, *32*, 1805864.
- (2) Shen, C.; Xu, S.; Xie, Y.; Sanghadasa, M.; Wang, X.; Lin, L. A review of on-chip micro supercapacitors for integrated self-powering systems. *J. Microelectromech. Syst.* **2017**, *26*, 949–965.
- (3) Lethien, C.; Le Bideau, J.; Brousse, T. Challenges and prospects of 3D micro-supercapacitors for powering the internet of things. *Energy Environ. Sci.* **2019**, *12*, 96–115.
- (4) Wu, Z.-S.; Feng, X.; Cheng, H.-M. Recent advances in graphene-based planar micro-supercapacitors for on-chip energy storage. *Natl. Sci. Rev.* **2014**, *1*, 277–292.
- (5) Da, Y.; Liu, J.; Zhou, L.; Zhu, X.; Chen, X.; Fu, L. Engineering 2D Architectures toward High-Performance Micro-Supercapacitors. *Adv. Mater.* **2019**, *31*, 1802793.
- (6) Qi, D.; Liu, Y.; Liu, Z.; Zhang, L.; Chen, X. Design of architectures and materials in in-plane micro-supercapacitors: current status and future challenges. *Adv. Mater.* **2017**, *29*, 1602802.

- (7) Sun, G.; Yang, H.; Zhang, G.; Gao, J.; Jin, X.; Zhao, Y.; Jiang, L.; Qu, L. A capacity recoverable zinc-ion micro-supercapacitor. *Energy Environ. Sci.* **2018**, *11*, 3367–3374.
- (8) Shao, Y.; Li, J.; Li, Y.; Wang, H.; Zhang, Q.; Kaner, R. B. Flexible quasi-solid-state planar micro-supercapacitor based on cellular graphene films. *Mater. Horiz.* **2017**, *4*, 1145–1150.
- (9) Liu, L.; Zhao, H.; Lei, Y. Advances on three-dimensional electrodes for micro-supercapacitors: a mini-review. *InfoMater.* **2019**, *1*, 74–84.
- (10) Liu, N.; Gao, Y. Recent progress in micro-supercapacitors with in-plane interdigital electrode architecture. *Small* **2017**, *13*, 1701989.
- (11) Du, Z.; Wood, D. L.; Daniel, C.; Kalnaus, S.; Li, J. Understanding limiting factors in thick electrode performance as applied to high energy density Li-ion batteries. *J. Appl. Electrochem.* **2017**, *47*, 405–415.
- (12) Iro, Z. S.; Subramani, C.; Dash, S. A brief review on electrode materials for supercapacitor. *Int. J. Electrochem. Sci.* **2016**, *11*, 10628–10643.
- (13) Tahir, M.; He, L.; Haider, W. A.; Yang, W.; Hong, X.; Guo, Y.; Pan, X.; Tang, H.; Li, Y.; Mai, L. Co-electrodeposited porous PEDOT–CNT microelectrodes for integrated micro-supercapacitors with high energy density, high rate capability, and long cycling life. *Nanoscale* **2019**, *11*, 7761–7770.
- (14) Muzaffar, A.; Ahamed, M. B.; Deshmukh, K.; Thirumalai, J. A review on recent advances in hybrid supercapacitors: Design, fabrication and applications. *Renewable Sustainable Energy Rev.* **2019**, *101*, 123–145.
- (15) Xu, S.; Dall'Agnesse, Y.; Wei, G.; Zhang, C.; Gogotsi, Y.; Han, W. Screen-printable microscale hybrid device based on MXene and layered double hydroxide electrodes for powering force sensors. *Nano Energy* **2018**, *50*, 479–488.
- (16) Wang, T.; Chen, H. C.; Yu, F.; Zhao, X.; Wang, H. Boosting the cycling stability of transition metal compounds-based supercapacitors. *Energy Storage Mater.* **2019**, *16*, 545–573.
- (17) Shao, B.; Liu, Z.; Zeng, G.; Wang, H.; Liang, Q.; He, Q.; Cheng, M.; Zhou, C.; Jiang, L.; Song, B. Two-dimensional transition metal carbide and nitride (MXene) derived quantum dots (QDs): synthesis, properties, applications and prospects. *J. Mater. Chem. A* **2020**, *8*, 7508–7535.
- (18) Borah, R.; Hughson, F.; Johnston, J.; Nann, T. On battery materials and methods. *Mater. Today Adv.* **2020**, *6*, 100046.
- (19) Kumar, K. S.; Choudhary, N.; Jung, Y.; Thomas, J. Recent advances in two-dimensional nanomaterials for supercapacitor electrode applications. *ACS Energy Lett.* **2018**, *3*, 482–495.
- (20) Chhowalla, M.; Shin, H. S.; Eda, G.; Li, L.-J.; Loh, K. P.; Zhang, H. The chemistry of two-dimensional layered transition metal dichalcogenide nanosheets. *Nat. Chem.* **2013**, *5*, 263–275.
- (21) Duan, X.; Wang, C.; Pan, A.; Yu, R.; Duan, X. Two-dimensional transition metal dichalcogenides as atomically thin semiconductors: opportunities and challenges. *Chem. Soc. Rev.* **2015**, *44*, 8859–8876.
- (22) Ng, V. M. H.; Huang, H.; Zhou, K.; Lee, P. S.; Que, W.; Xu, J. Z.; Kong, L. B. Recent progress in layered transition metal carbides and/or nitrides (MXenes) and their composites: synthesis and applications. *J. Mater. Chem. A* **2017**, *5*, 3039–3068.
- (23) Naguib, M.; Mochalin, V. N.; Barsoum, M. W.; Gogotsi, Y. 25th anniversary article: MXenes: a new family of two-dimensional materials. *Adv. Mater.* **2014**, *26*, 992–1005.
- (24) Anasori, B.; Lukatskaya, M. R.; Gogotsi, Y. 2D metal carbides and nitrides (MXenes) for energy storage. *Nat. Rev. Mater.* **2017**, *2*, 1–17.
- (25) Vellacheri, R.; Pillai, V. K.; Kurungot, S. Hydrrous RuO<sub>2</sub>-carbon nanofiber electrodes with high mass and electrode-specific capacitance for efficient energy storage. *Nanoscale* **2012**, *4*, 890–896.
- (26) Jabeen, N.; Xia, Q.; Savilov, S. V.; Aldoshin, S. M.; Yu, Y.; Xia, H. Enhanced pseudocapacitive performance of  $\alpha$ -MnO<sub>2</sub> by cation preinsertion. *ACS Appl. Mater. Interfaces* **2016**, *8*, 33732–33740.
- (27) Liu, Q.; Hu, Z.; Chen, M.; Zou, C.; Jin, H.; Wang, S.; Chou, S. L.; Dou, S. X. Recent Progress of Layered Transition Metal Oxide Cathodes for Sodium-Ion Batteries. *Small* **2019**, *15*, 1805381.
- (28) Zhong, Y.; Xia, X.; Shi, F.; Zhan, J.; Tu, J.; Fan, H. J. Transition metal carbides and nitrides in energy storage and conversion. *Adv. Sci.* **2016**, *3*, 1500286.
- (29) Tahir, M.; He, L.; Yang, W.; Hong, X.; Haider, W. A.; Tang, H.; Zhu, Z.; Owusu, K. A.; Mai, L. Boosting the electrochemical performance and reliability of conducting polymer microelectrode via intermediate graphene for on-chip asymmetric micro-supercapacitor. *J. Energy Chem.* **2020**, *49*, 224–232.
- (30) Guan, G.; Han, M. Y. Functionalized Hybridization of 2D Nanomaterials. *Adv. Sci.* **2019**, *6* (23), 1901837.
- (31) Ganguly, P.; Harb, M.; Cao, Z.; Cavallo, L.; Breen, A.; Dervin, S.; Dionysiou, D. D.; Pillai, S. C. 2D nanomaterials for photocatalytic hydrogen production. *ACS Energy Lett.* **2019**, *4*, 1687–1709.
- (32) Choi, W.; Choudhary, N.; Han, G. H.; Park, J.; Akinwande, D.; Lee, Y. H. Recent development of two-dimensional transition metal dichalcogenides and their applications. *Mater. Today* **2017**, *20*, 116–130.
- (33) Jiang, K.; Weng, Q. Miniaturized Energy Storage Devices Based on Two-Dimensional Materials. *ChemSusChem* **2020**, *13*, 1420–1446.
- (34) Cao, L.; Yang, S.; Gao, W.; Liu, Z.; Gong, Y.; Ma, L.; Shi, G.; Lei, S.; Zhang, Y.; Zhang, S. Direct laser-patterned micro-supercapacitors from paintable MoS<sub>2</sub> films. *Small* **2013**, *9*, 2905–2910.
- (35) Winchester, A.; Ghosh, S.; Feng, S.; Elias, A. L.; Mallouk, T.; Terrones, M.; Talapatra, S. Electrochemical characterization of liquid phase exfoliated two-dimensional layers of molybdenum disulfide. *ACS Appl. Mater. Interfaces* **2014**, *6*, 2125–2130.
- (36) Ji, Q.; Li, C.; Wang, J.; Niu, J.; Gong, Y.; Zhang, Z.; Fang, Q.; Zhang, Y.; Shi, J.; Liao, L.; Wu, X.; Gu, L.; Liu, Z.; Zhang, Y. Metallic vanadium disulfide nanosheets as a platform material for multifunctional electrode applications. *Nano Lett.* **2017**, *17*, 4908–4916.
- (37) Acerce, M.; Voiry, D.; Chhowalla, M. Metallic 1T phase MoS<sub>2</sub> nanosheets as supercapacitor electrode materials. *Nat. Nanotechnol.* **2015**, *10*, 313.
- (38) Khalil, A.; Liu, Q.; He, Q.; Xiang, T.; Liu, D.; Wang, C.; Fang, Q.; Song, L. Metallic 1T-WS<sub>2</sub> nanoribbons as highly conductive electrodes for supercapacitors. *RSC Adv.* **2016**, *6*, 48788–48791.
- (39) Wu, J.; Peng, J.; Yu, Z.; Zhou, Y.; Guo, Y.; Li, Z.; Lin, Y.; Ruan, K.; Wu, C.; Xie, Y. Acid-assisted exfoliation toward metallic sub-nanopore TaS<sub>2</sub> monolayer with high volumetric capacitance. *J. Am. Chem. Soc.* **2018**, *140*, 493–498.
- (40) Wang, C.; Wu, X.; Ma, Y.; Mu, G.; Li, Y.; Luo, C.; Xu, H.; Zhang, Y.; Yang, J.; Tang, X. Metallic few-layered VSe<sub>2</sub> nanosheets: high two-dimensional conductivity for flexible in-plane solid-state supercapacitors. *J. Mater. Chem. A* **2018**, *6*, 8299–8306.
- (41) Huang, J.; Pan, X.; Liao, X.; Yan, M.; Dunn, B.; Luo, W.; Mai, L. In situ monitoring of the electrochemically induced phase transition of thermodynamically metastable 1T-MoS<sub>2</sub> at nanoscale. *Nanoscale* **2020**, *12*, 9246–9254.
- (42) Xia, D. D.; Gong, F.; Pei, X.; Wang, W.; Li, H.; Zeng, W.; Wu, M.; Papavassiliou, D. V. Molybdenum and tungsten disulfides-based nanocomposite films for energy storage and conversion: A review. *Chem. Eng. J.* **2018**, *348*, 908–928.
- (43) Qin, J.; Das, P.; Zheng, S.; Wu, Z.-S. A perspective on two-dimensional materials for planar micro-supercapacitors. *APL Mater.* **2019**, *7*, 090902.
- (44) Haider, W. A.; Tahir, M.; He, L.; Yang, W.; Minhas-khan, A.; Owusu, K. A.; Chen, Y.; Hong, X.; Mai, L. Integration of VS<sub>2</sub> nanosheets into carbon for high energy density micro-supercapacitor. *J. Alloys Compd.* **2020**, *823*, 151769.
- (45) Xiong, T.; Su, H.; Yang, F.; Tan, Q.; Appadurai, P.; Afuwape, A.; Guo, K.; Huang, Y.; Wang, Z.; Balogun, M.-S. J. T. Harmonizing self-supportive VN/MoS<sub>2</sub> pseudocapacitance core-shell electrodes for boosting the areal capacity of lithium storage. *Mater. Today Energy* **2020**, *17*, 100461.
- (46) Wang, C.; Wu, X.; Xu, H.; Zhu, Y.; Liang, F.; Luo, C.; Xia, Y.; Xie, X.; Zhang, J.; Duan, C. VSe<sub>2</sub>/carbon-nanotube compound for all solid-state flexible in-plane supercapacitor. *Appl. Phys. Lett.* **2019**, *114*, 023902.

- (47) Choudhary, N.; Li, C.; Chung, H.-S.; Moore, J.; Thomas, J.; Jung, Y. High-performance one-body core/shell nanowire supercapacitor enabled by conformal growth of capacitive 2D WS<sub>2</sub> layers. *ACS Nano* **2016**, *10*, 10726–10735.
- (48) Wang, L.; Zhang, X.; Ma, Y.; Yang, M.; Qi, Y. Supercapacitor performances of the MoS<sub>2</sub>/CoS<sub>2</sub> nanotube arrays in situ grown on Ti plate. *J. Phys. Chem. C* **2017**, *121*, 9089–9095.
- (49) Li, J.; Shi, Q.; Shao, Y.; Hou, C.; Li, Y.; Zhang, Q.; Wang, H. Cladding nanostructured AgNWs-MoS<sub>2</sub> electrode material for high-rate and long-life transparent in-plane micro-supercapacitor. *Energy Storage Mater.* **2019**, *16*, 212–219.
- (50) Rantho, M.; Madito, M.; Ochai-Ejeh, F.; Manyala, N. Asymmetric supercapacitor based on vanadium disulfide nanosheets as a cathode and carbonized iron cations adsorbed onto polyaniline as an anode. *Electrochim. Acta* **2018**, *260*, 11–23.
- (51) Su, H.; Xiong, T.; Tan, Q.; Yang, F.; Appadurai, P.; Afuwape, A. A.; Balogun, M.; Huang, Y.; Guo, K. Asymmetric Pseudocapacitors Based on Interfacial Engineering of Vanadium Nitride Hybrids. *Nanomaterials* **2020**, *10*, 1141.
- (52) Moosavifard, S. E.; Shamsi, J.; Altafi, M. K.; Moosavifard, Z. S. All-solid state, flexible, high-energy integrated hybrid micro-supercapacitors based on 3D LSG/CoNi<sub>2</sub>S<sub>4</sub> nanosheets. *Chem. Commun.* **2016**, *52*, 13140–13143.
- (53) Zhang, P.; Wang, L.; Wang, F.; Tan, D.; Wang, G.; Yang, S.; Yu, M.; Zhang, J.; Feng, X. A Nonaqueous Na-Ion Hybrid Micro-Supercapacitor with Wide Potential Window and Ultrahigh Areal Energy Density. *Batteries Supercaps.* **2019**, *2*, 918–923.
- (54) Li, J.-C.; Gong, J.; Zhang, X.; Lu, L.; Liu, F.; Dai, Z.; Wang, Q.; Hong, X.; Pang, H.; Han, M. Alternate Integration of Vertically Oriented CuSe@FeOOH and CuSe@MnOOH Hybrid Nanosheets Frameworks for Flexible In-Plane Asymmetric Micro-supercapacitors. *ACS Appl. Energy Mater.* **2020**, *3*, 3692–3703.
- (55) Hart, J. L.; Hantanasirisakul, K.; Lang, A. C.; Anasori, B.; Pinto, D.; Pivak, Y.; van Omme, J. T.; May, S. J.; Gogotsi, Y.; Taheri, M. L. Control of MXenes' electronic properties through termination and intercalation. *Nat. Commun.* **2019**, *10*, 1–10.
- (56) Zhang, C. J.; Nicolosi, V. Graphene and MXene-based transparent conductive electrodes and supercapacitors. *Energy Storage Mater.* **2019**, *16*, 102–125.
- (57) Ling, Z.; Ren, C. E.; Zhao, M.-Q.; Yang, J.; Giammarco, J. M.; Qiu, J.; Barsoum, M. W.; Gogotsi, Y. Flexible and conductive MXene films and nanocomposites with high capacitance. *Proc. Natl. Acad. Sci. U. S. A.* **2014**, *111*, 16676–16681.
- (58) Lukatskaya, M. R.; Kota, S.; Lin, Z.; Zhao, M.-Q.; Shpigel, N.; Levi, M. D.; Halim, J.; Taberna, P.-L.; Barsoum, M. W.; Simon, P. Ultra-high-rate pseudocapacitive energy storage in two-dimensional transition metal carbides. *Nat. Energy* **2017**, *2*, 17105.
- (59) Sang, X.; Xie, Y.; Lin, M.-W.; Alhabeb, M.; Van Aken, K. L.; Gogotsi, Y.; Kent, P. R.; Xiao, K.; Unocic, R. R. Atomic Defects in Monolayer Titanium Carbide (Ti<sub>3</sub>C<sub>2</sub>T<sub>x</sub>) MXene. *ACS Nano* **2016**, *10*, 9193–9200.
- (60) Kurra, N.; Alhabeb, M.; Maleski, K.; Wang, C.-H.; Alshareef, H. N.; Gogotsi, Y. Bistacked titanium carbide (MXene) anodes for hybrid sodium-ion capacitors. *ACS Energy Lett.* **2018**, *3*, 2094–2100.
- (61) Lukatskaya, M. R.; Mashtalir, O.; Ren, C. E.; Dall'Agnese, Y.; Rozier, P.; Taberna, P. L.; Naguib, M.; Simon, P.; Barsoum, M. W.; Gogotsi, Y. Cation intercalation and high volumetric capacitance of two-dimensional titanium carbide. *Science* **2013**, *341*, 1502–1505.
- (62) Lim, Y.; Yoon, J.; Yun, J.; Kim, D.; Hong, S. Y.; Lee, S.-J.; Zi, G.; Ha, J. S. Biaxially stretchable, integrated array of high performance microsupercapacitors. *ACS Nano* **2014**, *8*, 11639–11650.
- (63) Liew, C.-W.; Ramesh, S.; Arof, A. K. Good prospect of ionic liquid based-poly (vinyl alcohol) polymer electrolytes for supercapacitors with excellent electrical, electrochemical and thermal properties. *Int. J. Hydrogen Energy* **2014**, *39*, 2953–2963.
- (64) Zheng, J.; Li, X.; Yu, Y.; Zhen, X.; Song, Y.; Feng, X.; Zhao, Y. Cross-linking copolymers of acrylates' gel electrolytes with high conductivity for lithium-ion batteries. *J. Solid State Electrochem.* **2014**, *18*, 2013–2018.
- (65) Zheng, S.; Zhang, C. J.; Zhou, F.; Dong, Y.; Shi, X.; Nicolosi, V.; Wu, Z.-S.; Bao, X. Ionic liquid pre-intercalated MXene films for ionogel-based flexible micro-supercapacitors with high volumetric energy density. *J. Mater. Chem. A* **2019**, *7*, 9478–9485.
- (66) Zhang, C.; Kremer, M. P.; Seral-Ascaso, A.; Park, S. H.; McEvoy, N.; Anasori, B.; Gogotsi, Y.; Nicolosi, V. Stamping of flexible, coplanar micro-supercapacitors using MXene inks. *Adv. Funct. Mater.* **2018**, *28*, 1705506.
- (67) Jiang, Q.; Kurra, N.; Maleski, K.; Lei, Y.; Liang, H.; Zhang, Y.; Gogotsi, Y.; Alshareef, H. N. On-Chip MXene Microsupercapacitors for AC-Line Filtering Applications. *Adv. Energy Mater.* **2019**, *9*, 1901061.
- (68) Weng, G. M.; Li, J.; Alhabeb, M.; Karpovich, C.; Wang, H.; Lipton, J.; Maleski, K.; Kong, J.; Shaulsky, E.; Elimelech, M. Layer-by-Layer Assembly of Cross-Functional Semi-transparent MXene-Carbon Nanotubes Composite Films for Next-Generation Electromagnetic Interference Shielding. *Adv. Funct. Mater.* **2018**, *28*, 1803360.
- (69) Liang, X.; Rangom, Y.; Kwok, C. Y.; Pang, Q.; Nazar, L. F. Interwoven MXene Nanosheet/Carbon-Nanotube Composites as Li-S Cathode Hosts. *Adv. Mater.* **2017**, *29*, 1603040.
- (70) Yu, C.; Gong, Y.; Chen, R.; Zhang, M.; Zhou, J.; An, J.; Lv, F.; Guo, S.; Sun, G. A Solid-State Fibriform Supercapacitor Boosted by Host-Guest Hybridization between the Carbon Nanotube Scaffold and MXene Nanosheets. *Small* **2018**, *14*, 1801203.
- (71) Cai, Y.; Shen, J.; Ge, G.; Zhang, Y.; Jin, W.; Huang, W.; Shao, J.; Yang, J.; Dong, X. Stretchable Ti<sub>3</sub>C<sub>2</sub>T<sub>x</sub> MXene/Carbon Nanotube Composite Based Strain Sensor with Ultrahigh Sensitivity and Tunable Sensing Range. *ACS Nano* **2018**, *12*, 56–62.
- (72) Zhou, Z.; Panatdasirisuk, W.; Mathis, T. S.; Anasori, B.; Lu, C.; Zhang, X.; Liao, Z.; Gogotsi, Y.; Yang, S. Layer-by-layer assembly of MXene and carbon nanotubes on electrospun polymer films for flexible energy storage. *Nanoscale* **2018**, *10*, 6005–6013.
- (73) Jiao, S.; Zhou, A.; Wu, M.; Hu, H. Kirigami Patterning of MXene/Bacterial Cellulose Composite Paper for All-Solid-State Stretchable Micro-Supercapacitor Arrays. *Adv. Sci.* **2019**, *6*, 1900529.
- (74) Li, H.; Hou, Y.; Wang, F.; Lohe, M. R.; Zhuang, X.; Niu, L.; Feng, X. Flexible all-solid-state supercapacitors with high volumetric capacitances boosted by solution processable MXene and electrochemically exfoliated graphene. *Adv. Energy Mater.* **2017**, *7*, 1601847.
- (75) Yan, J.; Ren, C. E.; Maleski, K.; Hatter, C. B.; Anasori, B.; Urbankowski, P.; Sarycheva, A.; Gogotsi, Y. Flexible MXene/graphene films for ultrafast supercapacitors with outstanding volumetric capacitance. *Adv. Funct. Mater.* **2017**, *27*, 1701264.
- (76) Yue, Y.; Liu, N.; Ma, Y.; Wang, S.; Liu, W.; Luo, C.; Zhang, H.; Cheng, F.; Rao, J.; Hu, X.; Su, J.; Gao, Y. Highly self-healable 3D microsupercapacitor with MXene-graphene composite aerogel. *ACS Nano* **2018**, *12*, 4224–4232.
- (77) Xie, Y.; Zhang, H.; Huang, H.; Wang, Z.; Xu, Z.; Zhao, H.; Wang, Y.; Chen, N.; Yang, W. High-voltage asymmetric MXene-based on-chip micro-supercapacitors. *Nano Energy* **2020**, *74*, 104928.
- (78) Couly, C.; Alhabeb, M.; Van Aken, K. L.; Kurra, N.; Gomes, L.; Navarro-Suárez, A. M.; Anasori, B.; Alshareef, H. N.; Gogotsi, Y. Asymmetric Flexible MXene-Reduced Graphene Oxide Micro-Supercapacitor. *Adv. Electron. Mater.* **2018**, *4*, 1700339.
- (79) Kalantar-zadeh, K.; Ou, J. Z.; Daeneke, T.; Mitchell, A.; Sasaki, T.; Fuhrer, M. S. Two dimensional and layered transition metal oxides. *Appl. Mater. Today* **2016**, *5*, 73–89.
- (80) Bahloul, A.; Nessark, B.; Briot, E.; Groult, H.; Mauger, A.; Zaghib, K.; Julien, C. Polypyrrole-covered MnO<sub>2</sub> as electrode material for supercapacitor. *J. Power Sources* **2013**, *240*, 267–272.
- (81) Ten Elshof, J. E.; Yuan, H.; Gonzalez Rodriguez, P. Two-Dimensional Metal Oxide and Metal Hydroxide Nanosheets: Synthesis, Controlled Assembly and Applications in Energy Conversion and Storage. *Adv. Energy Mater.* **2016**, *6*, 1600355.
- (82) Zhang, P.; Wang, F.; Yu, M.; Zhuang, X.; Feng, X. Two-dimensional materials for miniaturized energy storage devices: from individual devices to smart integrated systems. *Chem. Soc. Rev.* **2018**, *47*, 7426–7451.

(83) Patil, S. J.; Park, J. S.; Kim, Y. B.; Lee, D. W. A Quasi 2D Flexible Micro-Supercapacitor Based on  $\text{MnO}_2/\text{NiCo}_2\text{O}_4$  as a Miniaturized Energy-Storage Device. *Energy Technol.* **2018**, *6*, 1380–1391.

(84) Wu, H.; Jiang, K.; Gu, S.; Yang, H.; Lou, Z.; Chen, D.; Shen, G. Two-dimensional  $\text{Ni}(\text{OH})_2$  nanoplates for flexible on-chip micro-supercapacitors. *Nano Res.* **2015**, *8*, 3544–3552.

(85) Kurra, N.; Alhebshi, N. A.; Alshareef, H. N. Microfabricated pseudocapacitors using  $\text{Ni}(\text{OH})_2$  electrodes exhibit remarkable volumetric capacitance and energy density. *Adv. Energy Mater.* **2015**, *5*, 1401303.

(86) Han, J.; Lin, Y. C.; Chen, L.; Tsai, Y. C.; Ito, Y.; Guo, X.; Hirata, A.; Fujita, T.; Esashi, M.; Gessner, T. On-chip micro-pseudocapacitors for ultrahigh energy and power delivery. *Adv. Sci.* **2015**, *2*, 1500067.

(87) Haider, W. A.; He, L.; Mirza, H. A.; Tahir, M.; Khan, A. M.; Owusu, K. A.; Yang, W.; Wang, Z.; Mai, L. Bilayered microelectrodes based on electrochemically deposited  $\text{MnO}_2/\text{polypyrrole}$  towards fast charge transport kinetics for micro-supercapacitors. *RSC Adv.* **2020**, *10*, 18245–18251.

(88) Wang, Y.; Zhang, Y.-Z.; Gao, Y.-Q.; Sheng, G.; Johan, E. Defect engineering of  $\text{MnO}_2$  nanosheets by substitutional doping for printable solid-state micro-supercapacitors. *Nano Energy* **2020**, *68*, 104306.

(89) Gong, J.; Li, J.-C.; Yang, J.; Zhao, S.; Yang, Z.; Zhang, K.; Bao, J.; Pang, H.; Han, M. High-performance flexible in-plane micro-supercapacitors based on vertically aligned  $\text{CuSe@Ni}(\text{OH})_2$  hybrid nanosheet films. *ACS Appl. Mater. Interfaces* **2018**, *10*, 38341–38349.

(90) Wang, Y.; Zhang, Y.-Z.; Dubbink, D.; Johan, E. Inkjet printing of  $\delta\text{-MnO}_2$  nanosheets for flexible solid-state micro-supercapacitor. *Nano Energy* **2018**, *49*, 481–488.

(91) Tang, C.; Xiong, F.; Yao, X.; Tan, S.; Lan, B.; An, Q.; Luo, P.; Mai, L. Hierarchical  $\text{Mn}_3\text{O}_4/\text{graphene}$  microflowers fabricated via a selective dissolution strategy for alkali-metal-ion storage. *ACS Appl. Mater. Interfaces* **2019**, *11*, 14120–14125.

(92) Yue, Y.; Yang, Z.; Liu, N.; Liu, W.; Zhang, H.; Ma, Y.; Yang, C.; Su, J.; Li, L.; Long, F.; Zou, Z.; Gao, Y. A flexible integrated system containing a microsupercapacitor, a photodetector, and a wireless charging coil. *ACS Nano* **2016**, *10*, 11249–11257.

(93) Zheng, S.; Lei, W.; Qin, J.; Wu, Z.-S.; Zhou, F.; Wang, S.; Shi, X.; Sun, C.; Chen, Y.; Bao, X. All-solid-state high-energy planar asymmetric supercapacitors based on all-in-one monolithic film using boron nitride nanosheets as separator. *Energy Storage Mater.* **2018**, *10*, 24–31.

(94) Qin, J.; Wang, S.; Zhou, F.; Das, P.; Zheng, S.; Sun, C.; Bao, X.; Wu, Z.-S. 2D mesoporous  $\text{MnO}_2$  nanosheets for high-energy asymmetric micro-supercapacitors in water-in-salt gel electrolyte. *Energy Storage Mater.* **2019**, *18*, 397–404.

(95) Sun, Y.; Guo, S.; Zhou, H. Adverse effects of interlayer-gliding in layered transition-metal oxides on electrochemical sodium-ion storage. *Energy Environ. Sci.* **2019**, *12*, 825–840.

(96) Zhang, Q.; Zhang, J.; Zhou, Z.; Wei, L.; Yao, Y. Flexible quasi-solid-state 2.4 V aqueous asymmetric microsupercapacitors with ultrahigh energy density. *J. Mater. Chem. A* **2018**, *6*, 20145–20151.

(97) Wang, S.; Wu, Z.-S.; Zhou, F.; Shi, X.; Zheng, S.; Qin, J.; Xiao, H.; Sun, C.; Bao, X. All-solid-state high-energy planar hybrid micro-supercapacitors based on 2D VN nanosheets and  $\text{Co}(\text{OH})_2$  nanoflowers. *NPJ. 2D Mater. Appl.* **2018**, *2*, 1–8.